الجمهورية الجزائرية الديمقراطية الشعبية
People's Democratic Republic of Algeria
وزارة التعليم العالي والبحث العلمي
Ministry of Higher Education and Scientific Research
جامعة محمد بوضياف – المسيلة
Mohamed Boudiaf University - M'Sila
كلية التكنولوجيا
Faculty of Technology
قسم الإلكتـرونيك
Department of Electronics

Master's Thesis

Field: Science and Technology
Specialty: Electronics
OPTION : MICROÉLECTRONIQUE

Thesis Title

Modelling and Simulation of Photovoltaic Modules with Integrated Common Faults

Proposed and Directed by:
DRIF Mahmoud

Carried out by:
MSELES LAZHER

Order Number:

Graduation: June 2025

TABLE OF CONTENT

Chapter 3: Modelling and simulation

LIST OF FIGURES

LIST OF TABLES

INTRODUCTION:

In recent decades, photovoltaic (PV) systems have become one of the most widely adopted renewable energy technologies due to their environmental benefits, scalability, and the global abundance of solar energy. These systems convert sunlight directly into electricity using semiconductor materials, providing a clean and sustainable alternative to fossil fuels. Their integration into both residential and large-scale energy infrastructures has significantly increased, driven by technological advancements and decreasing production costs.

In utility-scale PV installations, a solar power plant may comprise hundreds or even thousands of photovoltaic panels. The quality and stability of the energy produced are directly influenced by the performance of each individual cell. A major challenge in these systems lies in monitoring this vast array of cells to ensure consistent and efficient operation. Although PV systems are generally more reliable than many other energy systems, they remain vulnerable to faults that can degrade their performance. Research has shown that PV system reliability is strongly influenced by the quality of materials used in panel construction and by environmental factors such as temperature, humidity, and solar radiation.

Despite their advantages and relative reliability, PV systems are not immune to faults and performance degradation. Several studies have demonstrated that various internal and external factors—such as material aging, manufacturing defects, thermal stress, humidity, and environmental conditions—can lead to significant anomalies in PV operation. Among the most frequently encountered faults are partial shading, open-circuit or short-circuit faults, degradation of photovoltaic cells, and issues related to bypass or blocking diodes. These faults may result in reduced energy output, hotspots, system instability, or, in severe cases, total shutdown of the PV generator.

When a PV generator operates under faulty conditions, performance drops and, in extreme cases, the system may become completely inoperative. These outcomes not only reduce energy production but also negatively affect economic returns, especially when accounting for the cost of maintenance and system restoration. Consequently, fault detection and localization have become essential aspects of PV system management. The scientific literature provides numerous algorithms and diagnostic methods, applicable to both general industrial systems and PV-specific applications. These tools are designed to address different stages of fault analysis—detection, localization, and identification—and depend on the availability of sufficient operational data.

To maintain optimal performance and ensure long-term reliability, early detection and accurate diagnosis of such faults are essential. This has led to the development of numerous modeling and simulation techniques aimed at reproducing fault scenarios under controlled conditions. Fault modeling plays a critical role in understanding system behavior under abnormal conditions, facilitating the design of effective fault detection, localization, and mitigation strategies

This thesis is structured into three chapters:

- **Chapter One** presents a general introduction to photovoltaic energy conversion, covering the conversion chain in PV systems, the photovoltaic effect, the structure of solar cells, and various operating modes.
- **Chapter Two** explores the primary faults affecting PV generators and reviews a range of diagnostic techniques used for fault detection and localization.
- **Chapter Three** details the simulation results obtained from simplified PV system models, aiming to identify and classify the various faults analyzed in this study.

Chapter 1

Chapter 1: State of the Art on Photovoltaic Energy Conversion

I. Introduction

Photovoltaic (PV) systems have emerged as a key technology in the transition toward renewable energy, offering an environmentally friendly and sustainable solution to the growing global demand for electricity. By converting solar radiation directly into electrical energy through the photovoltaic effect, these systems provide clean power with minimal environmental impact. Their deployment ranges from small-scale residential installations to large utility-scale solar farms, thanks to advancements in materials, efficiency, and cost reduction.

However, like all technical systems, PV installations are subject to a range of operational issues that can affect their performance and reliability. Despite being considered robust and low-maintenance, PV systems are vulnerable to various types of faults stemming from environmental influences (such as temperature variations, humidity, and dust), aging of components, manufacturing defects, or improper installation. The most frequently observed faults include partial shading, open-circuit and short-circuit failures, degradation of solar cells, and malfunctions of bypass or blocking diodes. These anomalies can lead to reduced energy production, the formation of hotspots, efficiency loss, or even complete system failure if not promptly addressed.

To address these challenges, fault modeling has become an essential tool in the development of diagnostic and monitoring strategies. By simulating different fault scenarios, researchers and engineers can better understand the impact of each fault on system behavior. This allows for the design of more accurate fault detection, localization, and classification algorithms, ultimately improving system reliability, reducing maintenance costs, and maximizing energy yield.

This chapter introduces the fundamental structure and functioning of PV systems, highlights the most common faults encountered during operation, and presents the role of fault modeling in system analysis and diagnostic development.

II. Photovoltaic Conversion

The operating principle of a solar cell is based on the photovoltaic effect, which enables the direct conversion of sunlight into electricity. This process involves the generation and movement of positive and negative electric charges within a semiconductor material, typically silicon. A standard photovoltaic cell consists of two silicon layers: one n-type, enriched with excess electrons, and the other p-type, characterized by a deficiency of electrons (i.e., an abundance of "holes").

When these two layers are brought into contact, electrons from the n-type region naturally diffuse into the p-type region, and vice versa. This migration of charges creates a depletion zone at the junction, where an internal electric field is established. This field pushes electrons back toward the n-type side and holes toward the p-type side, forming a potential barrier.

By integrating metallic contacts on both sides of this junction, the structure functions as a diode. When the cell is exposed to light, photons with energy equal to or greater than the semiconductor's bandgap transfer their energy to the atoms. This excites electrons from the valence band to the conduction band, generating electron-hole pairs.

If an external circuit is connected across the terminals of the cell (as illustrated in Figure 1.1), the internal electric field drives electrons toward the external circuit from the n-side and holes toward the p-side, producing a potential difference and enabling electric current to flow.

This p-n junction thus exhibits the electrical behavior of a conventional silicon diode, but under illumination, it additionally generates a photocurrent that is independent of the voltage across the cell and is directly proportional to both the incident light intensity and the surface area of the cell.

II.1. Photovoltaic Effect

The photovoltaic effect, often abbreviated as PV, is a physical phenomenon observed in certain materials known as semiconductors, with silicon being the most commonly used. This effect forms the fundamental operating principle of photovoltaic cells and occurs in three main stages:

1. **Light absorption** by the semiconductor material of the PV cell.
2. **Energy transfer** from incident photons to charge carriers (electrons and holes), enabling their excitation.
3. **Charge collection** through an internal electric field, which directs the separated charges toward external terminals, resulting in the generation of electrical current.

This sequence of events enables the direct conversion of solar energy into electricity in photovoltaic systems.

.

II.1.1. General Principle

The formation of a p-n junction through the doping of silicon constitutes the fundamental operating principle of a solar cell. This junction creates a potential barrier within the semiconductor, which enables the separation of charge carriers—electrons and holes—generated by the absorption of light within the material.

When the junction is formed, electrons diffuse naturally from the n-type region toward the p-type region, while holes diffuse in the opposite direction. This movement, driven by the alignment of the Fermi levels, tends to establish thermodynamic

equilibrium. At the interface of the junction, this redistribution of charges forms a dipole, which gives rise to an internal electric field. This field acts as a barrier, opposing any further displacement of charges.

Applying a forward bias to the junction reduces the height of the potential barrier, thereby weakening the internal electric field and allowing charge carriers to cross the junction more easily. Conversely, a reverse bias increases the height of the barrier and reinforces the electric field, limiting the flow of carriers.

The current-voltage relationship of an ideal diode under dark conditions (i.e., without illumination) is described by the following equation:

$$I = I_0 \left(exp\ (\frac{qV}{nKT}) - 1 \right) \tag{1.1}$$

Where:

- **I□** is the **diode reverse saturation current** (A),
- **n** is the **ideality factor** of the diode (dimensionless),
- **k** is the **Boltzmann constant** (1.38×10^{-23} J/K),
- **q** is the **elementary charge** (1.602×10^{-1}□ C),
- **T** is the **absolute temperature** in Kelvin (K).

The thermodynamic equilibrium of the junction is disturbed when charge carriers are introduced either through external biasing or illumination. Under such conditions, the system enters a state known as quasi-equilibrium, where the carrier distributions no longer follow a single Fermi level.

To describe this state more accurately, two separate quasi-Fermi levels are introduced:

- **EF□** for electrons, and
- **EF□** for holes.

These quasi-Fermi levels provide a simplified and effective way to represent carrier behavior under non-equilibrium conditions, particularly in illuminated or forward-biased junctions [4].

II.1.2. Solar Cell

1. A wide range of technologies are available for the fabrication of photovoltaic cells, although many are still in the research and development phase. Currently, the majority of industrial-scale production relies on **crystalline silicon (c-Si)**, which accounted for approximately **80% of the market share in 2010**.
2. **Amorphous silicon (a-Si)**, once a favored technology due to its lower production costs, has seen a decline in market presence in recent years, particularly as **thin-film technologies** have gained traction. For example, the **cadmium telluride (CdTe)** technology experienced a significant market increase, rising from **2% in 2005 to 13% in 2010**.
3. Other thin-film technologies, such as **CIGS** (Copper Indium Gallium Selenide), along with several **emerging next-generation PV technologies**, are also progressing steadily and hold promising potential for future market growth and diversification.

II.1.3. Solar Cell and Different Operating Modes

A solar cell is typically designed to operate as a **generator**, converting solar energy into electrical power to supply an external load. However, under certain conditions, when interconnected with other cells, the same solar cell can function as a **receiver**, absorbing energy provided by the other cells. The electrical characteristics of a solar cell under different operating regimes (characteristics in three quadrants) are illustrated in Figure 1.1.

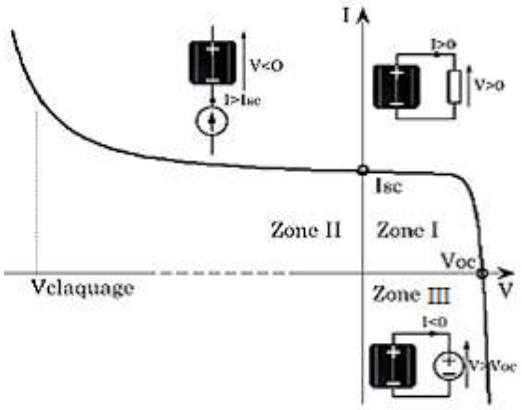

Figure 1.1. I-V Characteristics of a Solar Cell Under Different Operating Regimes

In this figure, two important operating points are noticeable: the **short-circuit current (Isc)** and the **open-circuit voltage (Voc)**. As the name suggests, the short-circuit current is the current when the cell is short-circuited. This current is directly proportional to the surface area of the cell that captures light, and for any given surface, it depends on the intensity of light absorbed by the cell. The open-circuit voltage is the voltage across the cell's terminals when no current is flowing. For a crystalline silicon cell, this value typically ranges around **0.6 V**.

These two points, **Voc** and **Isc**, define the cell's operation within three distinct zones:

- **Zone I**: This corresponds to the cell operating as a **generator**, with $\mathbf{0 \leq I \leq Isc}$ and $\mathbf{0 \leq V \leq Voc}$. This is the cell's normal operating regime, where it supplies power to an external load.
- **Zone II**: In this zone, the cell operates as a **receiver**, with $\mathbf{I > Isc}$ and $\mathbf{V < 0}$. When the current forced through the cell by an external circuit exceeds the short-circuit current, the cell produces a negative voltage across its terminals. If the current continues to grow, the cell could be damaged if the voltage reaches a threshold known as the **breakdown voltage**. Experimental studies on various crystalline cells have shown that the breakdown voltage typically ranges from **-10 V to -30 V**.
- **Zone III**: This zone also corresponds to the cell operating as a **receiver**, but now with $\mathbf{I < 0}$ and $\mathbf{V > Voc}$. When the voltage across the cell exceeds the open-circuit voltage, an **inverse current** begins to flow through the cell. If this reverse current surpasses a certain limit, the cell will suffer **irreversible damage**.

II.1.4. Solar Cell Model

A commonly used example is the **single-diode model** (Figure 1.2), which is widely adopted due to its simplicity, fast simulation capabilities, and acceptable accuracy in representing the behavior of a solar cell.

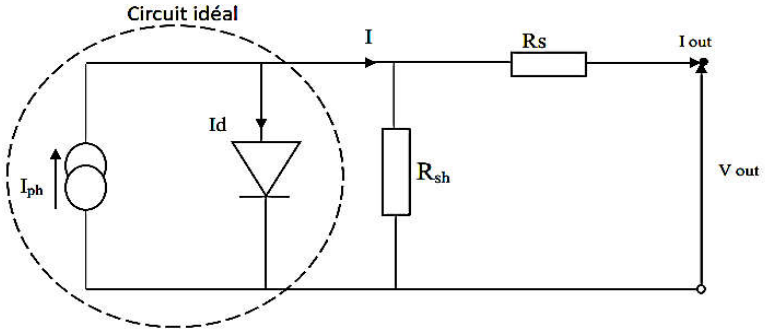

Figure 1.2. Equivalent Electrical Circuit of the Single-Diode Model

This model includes a **current source (Iph)**, which represents the solar irradiance received by the cell, and a **diode** in parallel that models the PN junction behavior. The **series resistance (Rs)** accounts for ohmic losses in the materials, metallic contacts, and semiconductor connections. The **parallel (or shunt) resistance (Rsh)** represents leakage currents that occur between the front and back surfaces of the solar cell.

The equation of the single-diode model of the PV cell is given by the following expression:

$$I = I_{ph} - I_o \left(\exp\left(\frac{V + I\,R_s}{n\,V_t} \right) - 1 \right) - \frac{V + I\,R_s}{R_{sh}} \qquad (1.1)$$

a) Photocurrent

The current **Iph**, known as the **photocurrent**, depends on **temperature**, **solar irradiance**, and the **temperature coefficient of the short-circuit current** (typically denoted as **α**), which is usually provided by the manufacturer. The photocurrent **Iph** can be expressed as follows:

$$I_{ph} = \left(I_{ph.STC} + \alpha\,(T_c - 25) \right) \frac{G}{G_{STC}} \qquad (1.2)$$

Where:

- Iph,STCI_{ph,STC}Iph,STC: Photocurrent under Standard Test Conditions (1000 W/m², AM1.5) [A]
- α\alphaα: Temperature coefficient of the short-circuit current [A/°C]
- TcT_cTc: Cell temperature [°C]
- GGG: Solar irradiance received by the cell [W/m²]
- GSTCG_{STC}GSTC: Solar irradiance under Standard Test Conditions [W/m²]

The cell temperature can be expressed as a function of the ambient temperature using the following equation:

$$T_c = T_a + \frac{NOCT - 20}{800}\,G \qquad (1.3)$$

Where:

b) TCT_CTC: Cell temperature [°C]
c) TaT_aTa: Ambient temperature [°C]
d) **NOCT**: Nominal Operating Cell Temperature (the typical operating temperature of the solar cell under standard conditions)
e) Diode Saturation Current

he diode's reverse saturation current, which represents the asymptotic value of the current III under reverse bias, depends on the temperature and the bandgap energy of the solar cell material.

$$I_o = I_{o.ref}\left(\frac{T_c}{T_{c.STC}}\right)^3 \exp\left(\frac{q\,E_g}{m\,T_{c.STC}}\right)\left(\frac{1}{T_{c.STC}} - \frac{1}{T_c}\right) \quad (1.4)$$

Where:

- I0: Reverse saturation current at cell temperature Tc
- I0,ref: Reference reverse saturation current
- Eg: Bandgap energy. For silicon, it is equal to 1.12 eV
- The thermal voltage Vtis given by the following equation:

$$V_t = n\frac{kT}{q} \quad (1.5)$$

- k: Boltzmann constant
- n: Diode ideality factor
- q: Electron charge

II.1.5. Performance Parameters of a Solar Cell

The current-voltage (I-V) characteristic of an illuminated solar cell takes the shape shown in Figure 1.4, where the voltage across the load is swept from zero to the open-circuit voltage Voc.

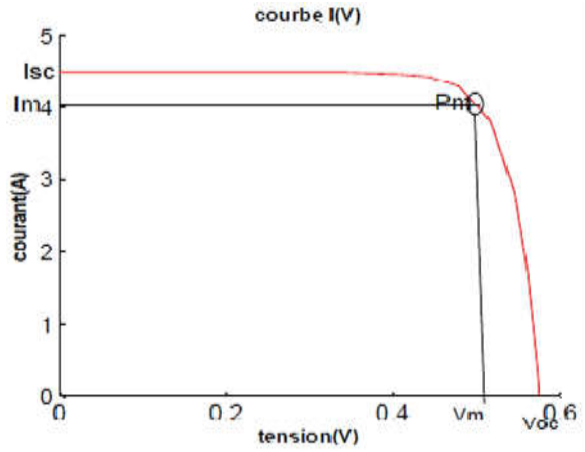

Figure 1.3. I-V Characteristic of a Solar Cell

Where:

- Im: Current delivered by the cell at the maximum power point Pm.
- Vm: Voltage across the cell at the maximum power point Pm.

a) Open-Circuit Voltage

It represents the voltage across the cell under illumination with no load connected (V = Voc, I = 0). It is given by the following expression:

$$V_{oc} = n\,V_t \ln\left(\frac{I_{ph}}{I_o} + 1\right) \tag{1.6}$$

f) Short-Circuit Current

g) It represents the current delivered by the cell when the voltage across its terminals is zero (V = 0). It is given by the following expression:

$$I_{sc} = \left(I_{ph.STC} + \propto (T_c - 25)\right)\frac{G}{G_{STC}} \tag{1.7}$$

h) Delivered Power

The power delivered by the cell is the product of current and voltage, P= I×V.

$$P = I.V = \left[I_{ph} - I_o\left(\exp\left(\frac{V + I\,R_s}{n\,V_t}\right) - 1\right) - \frac{V + I\,R_s}{R_{sh}}\right].V \tag{1.8}$$

This power reaches its maximum, P= Pm, when the derivative $\frac{\partial P}{\partial V} = \mathbf{0}$

i) Fill Factor

The fill factor is defined as the ratio between the maximum power and the product of Voc and Isc

$$FF = \frac{P_m}{V_{oc}I_{sc}} = \frac{I_m V_m}{V_{oc}I_{sc}} \tag{1.9}$$

j) Conversion Efficiency

The efficiency, η, of PV cells refers to the power conversion efficiency. It is defined as the ratio between the maximum power delivered by the cell and the incident light power Pinc:

$$\eta = \frac{P_m}{P_{inc}} = \frac{I_m V_m}{G\,A_c} \tag{1.10}$$

Where Ac is the active area of the cell (in m²) and G is the incident irradiance (in W/m²).

II.2. Photovoltaic Module

Solar cells are typically connected in series within commercially available photovoltaic modules. Connecting the cells in series increases the overall voltage while the current remains constant. A standard photovoltaic module usually consists of 36 or 72 interconnected cells. Figure 1.5 illustrates a module comprising 36 cells connected in series.

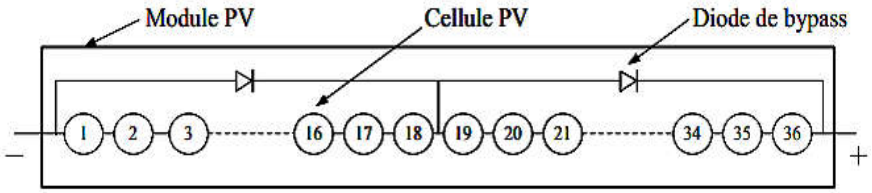

Figure 1.4. Series connection of solar cells in a PV module

The I-V characteristics and their behavior in series and parallel connections are shown in Figures 1.6 and 1.

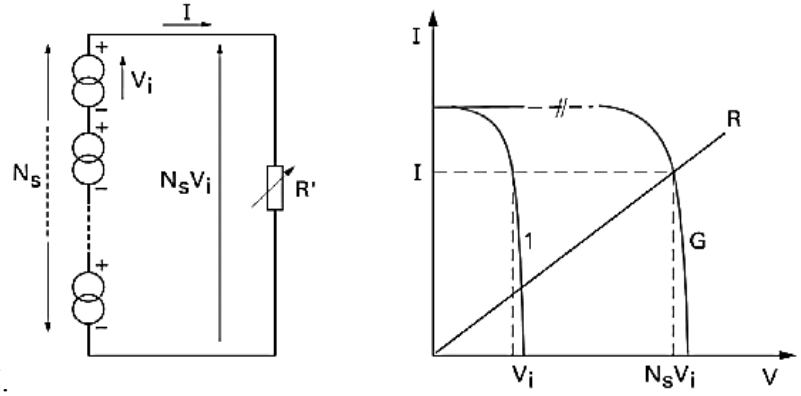

7.

Figure 1.5. I-V Characteristic of Solar Cells Connected in Series

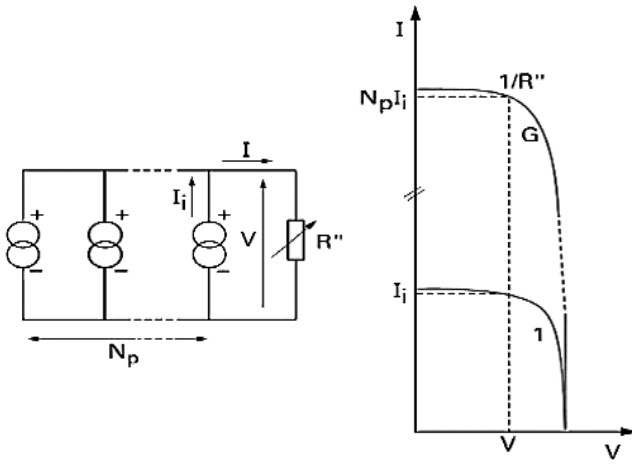

Figure 1.6. I-V Characteristic of Solar Cells Connected in Parallel

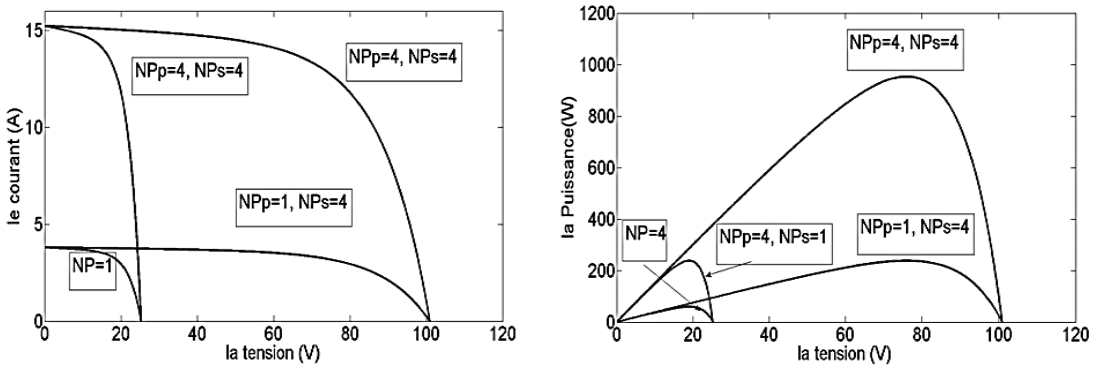

Figure 1.7. I-V and P-V characteristics of a mixed (series-parallel) connection. ***NPs***is the number of modules connected in series, and ***NPp***is the number of parallel module strings.

To achieve the desired current and voltage levels, it is often necessary to use a hybrid configuration of PV modules, combining both series and parallel connections. Figure 1.8 illustrates the I-V and P-V characteristics of such a mixed arrangement.

II.2.1.Protection of a Photovoltaic Generator Against Overcurrent

A photovoltaic generator, like any other electrical power generator, must be protected against overcurrent's as well as other types of issues that may affect its operation.

II.2.2. Protection Against the Partial Shading Effect

Partial shading of a solar cell forces it to operate in the third quadrant (Q3, see Figure I-7), meaning the polarity of the cell's voltage is reversed and rises to the junction's reverse voltage threshold (UC ≈ -15 V to -25 V). The power absorbed by the shaded cells significantly exceeds the power they normally dissipate, causing hot spots.
These hot spots can cause permanent damage to the PV module. Overcurrent protection is ineffective in this case because the increased power dissipation is due to the appearance of a reverse voltage in the affected cell, rather than a significant rise in the short-circuit current (Isc).

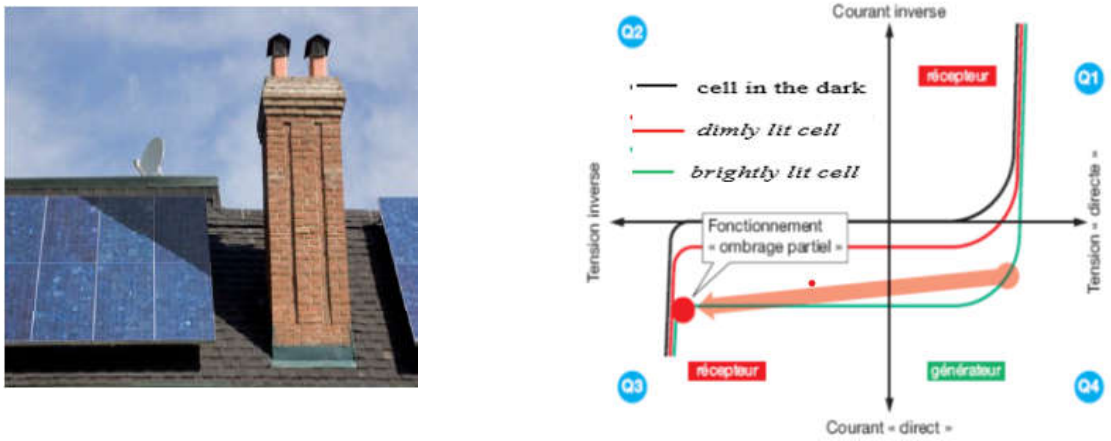

(a) (b)

Figure 1.8. (a) Shading of modules caused by a house chimney, (b) Operation of the cell in the third quadrant of the I-V characteristic due to shading.

A bypass diode allows the current from the other series-connected cells to flow around the shaded cell (Figure 1.10). This prevents reverse voltage stress and the resulting hot spots caused by shading, enabling the unshaded cells in the string to continue generating their normal current instead of being limited to the reduced current provided by the shaded cell.

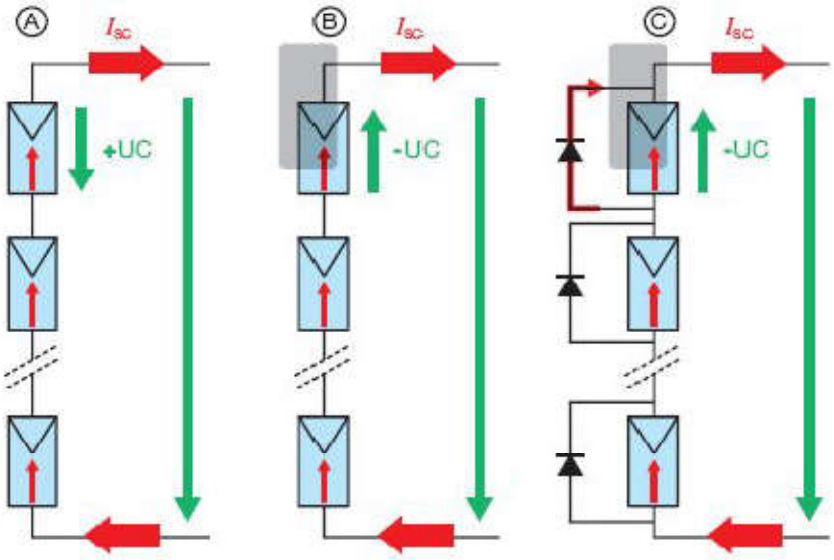

Figure 1.9. Photovoltaic system in:(a) normal operation,(b) presence of shading causing cell overheating,(c) protection by the installation of a bypass diode.

II.2.3. **Protection Against Reverse Currents**

The sizing of the string cables heavily depends on voltage drops; the acceptable current ratings for protecting the wiring against overloads are generally met automatically and usually do not require additional protective devices for this purpose. The main criterion for selecting fuses is the maximum reverse current (IRM) that the module can temporarily withstand until the chosen protective fuse interrupts the fault current caused by a defect.

Since our work focuses solely on faults leading to a reduction in power output, we concentrate exclusively on the components used to protect the photovoltaic generator

III. Conclusion

The study of photovoltaic systems highlights the critical importance of understanding both the electrical behavior of solar cells and the protective measures required to ensure their reliable operation. Accurate modeling of the solar cell and its components enables better prediction of performance under various conditions. Additionally, implementing appropriate protections against faults such as overcurrent's, shading effects, and reverse currents is essential to maintain the longevity and efficiency of the photovoltaic generator. Overall, the integration of these considerations contributes significantly to optimizing the design and operation of solar energy systems.

Chapter 2

Operating faults of a PV module and diagnostic techniques

I. Introduction

Like any electrical or electronic system, a photovoltaic (PV) solar system may experience failures or degradation during operation. Several faults or anomalies can affect the PV generator (a set of PV modules). These faults significantly impact the performance of the PV generator, oftenleading to changes in it's I-Vcharacteristics. The objective of this chapter is to present the different operating faults of a PV generator and the corresponding diagnostic techniques.

II. Operating Faults of a PV Generator

To better understand the subject, we define a few key concepts in the following points:

- **Fault**: A fault is defined as any deviation between the observed characteristic of the device and its theoretical characteristic.
- **Diagnosis**: The process of determining the type, magnitude, location, and time of occurrence of a fault (completes detection by adding isolation and identification).
- **Failure**: A permanent interruption of the system's ability to perform a required function under specified operating conditions.
- **Symptom**: A change in the observed quantity from normal behavior.
- **Detection**: It consists in recognizing that a device is operating in a faulty mode based on knowledge of certain characteristics.
- **Localization**: It consists in determining the physical or functional causes of a fault, that is, identifying the component(s) responsible for the fault.

Table 2.1 presents the main faults and anomalies, classified according to their location within a PV generator.

Table 2.1: Different Faults of a PV Generator

Component	Diagnostic Fault
PV Generator	• Leaves, bird droppings, pollution, sand, snow, etc. • Cell degradation, cracking, cell overheating • Moisture penetration, degradation of interconnections • Corrosion of intercell connections • Modules with different performance levels • Torn off or broken module • Short-circuited modules, reversed modules
Junction Box	• Open circuit in the electrical circuit • Short circuit in the electrical circuit • Connection failure • Corrosion of connections
Wiring and Connector	• Open circuit • Short circuit • Incorrect wiring (reversed module) • Contact corrosion • Electrical circuit break
Protection (bypass diode and blocking diode)	• Diode damage • Missing or non-functional diodes • Reversed diode polarity during installation

II.1 Classification of PV Generator Faults

Several classifications of faults are mentioned in the literature. In our work, we have chosen the classification based on the level at which the fault occurs and the stage in which it appears, as well as whether it affects the behavior of the component at that stage (cell, modulesor array). Based on the proposed 'PV fault tree' (Figure II-1), we will detail in the following the typical PV faults related to the three levels.

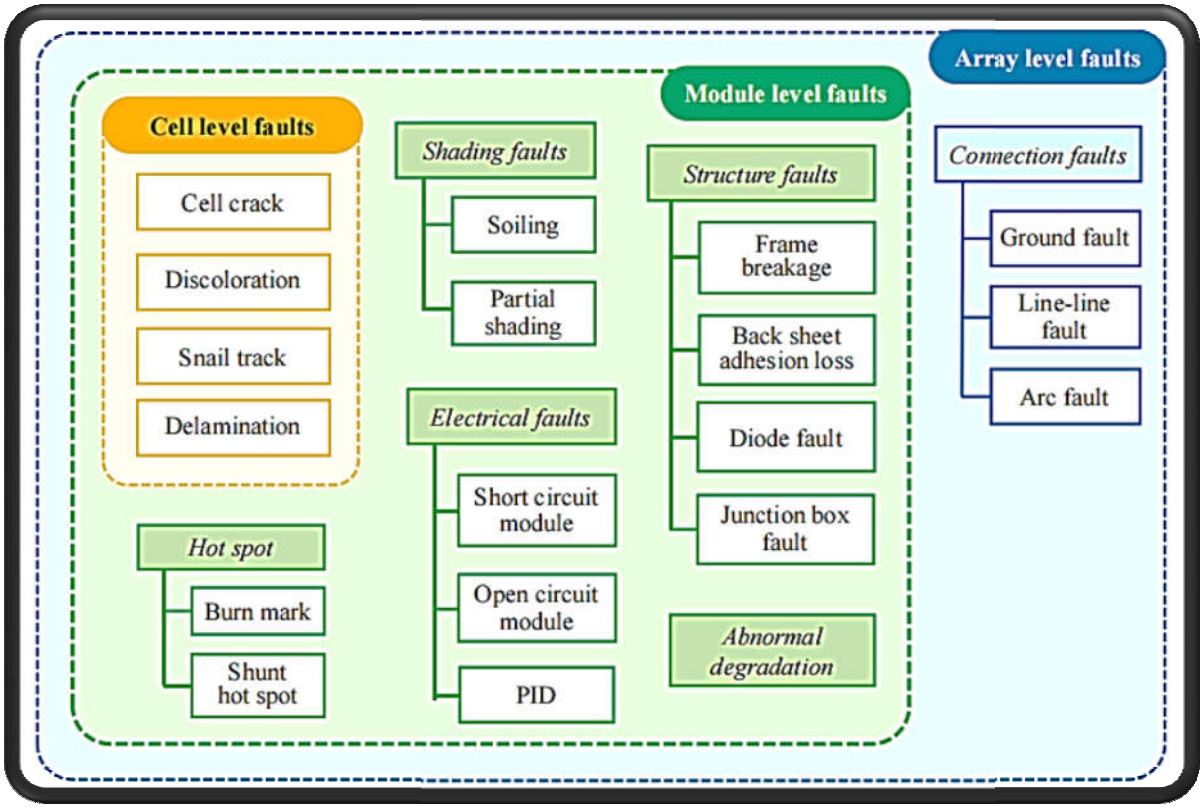

Figure.2.1 Classification of Photovoltaic Array Faults

II.1.1 Cell-level faults:

Cell-level faults referto the PV faults affecting a single PV cell. These faults mightspread over adjacent areas over time, but generally will not cause an overall impact onthe whole surface of the PV module. These faults are introduced in table II.1 with corresponding image.

Fault	Description	Example
Cell crack	Cell cracks are the cracks induced by mechanical stress in the silicon substrate of the photovoltaic cells, which usually are invisible by naked eyes. Itcould rise from the production, transport, installation, and operation stages. The shape of crack has different lengths and orientation in one solar cell. Cell crack could lead to different levels of power loss, which depends on the 'inactive' area of the cell.	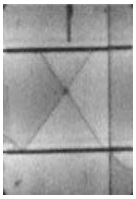

Discoloration	Discoloration is generally related to the PV modules using EVA (Ethylene Vinyl Acetate) as the encapsulant material. Discoloration refers to the yellowing or browning of PV cells. It causes a change in the transmission of solar irradiance reaching the cell surface and consequently a reduction in production. Nowadays, this fault is greatly eased for the PV modules with new encapsulant material. For example, forthermoplastic polyolefin, the discoloration rate is reported around 9 times lower.	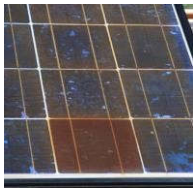
Snail track	Snail track is grey/black discoloration of the silver paste of the front metallization of screen-printed solar cells. The discoloring typically occurs 3 months to 1 year after installation of the PV modules. The origin of snail track is not clear, may be due to silver particles which contains sulfur, phosphorus, or carbon. The growth speed of the snail track discoloration may be very slow, or it saturates directly after the first occurrence.	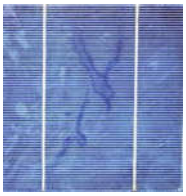
Delamination	Delamination is the adhesion loss between the glass, encapsulant, active layer and back layer. For thin-film PV type, the Transparent conductive oxide (TCO) may as well delaminate from the adjacent glass layer. Bubble is also a form of delamination. Delamination will lead to opticalreflection and therefore cause the decrease in power output. It also causes moisturepenetration, which then leads to variouschemical and physical degradation.	

Table 2.2:Cell-level faults

II.1.2 Module level-faults

At the module level, the common PV faults could be categorized into shading, structure, and electrical faults. Further, hot spot, as a joint result of diode fault and partial shading or mismatch, is also a type of module-level fault. Detailed presentation of these faults is given in Table II-2.

Fault	Description	Example
Shading/soiling	Shading and partial shading (PS) are usually caused by building, tree, moving cloud and so on; Soiling refers to snow, dirt, dust, and other particles that cover the surface of PV module. Shading/soiling could be classified into hard or soft type, or permanent/temporary type.	
Frame breakage	The main cause of frame breakage is heavy snow load, which will creep downhill and intrude into the space between frame and glass. It leads to deformation of module, detachment of frame from the PV glass, which will result in power loss.	
Back sheet adhesion loss	Depending on the material type of back sheet adopted in PV, causes for back sheet adhesion loss are similar to that of delamination, including temperature, moisture, mechanical stress, etc. It results in isolation default, therefore, increase the exposure to active electrical component, especially when happen near a junction box or edge of module.	
Junction box fault	Observed junction box fault includes poor fixing, bad wiring, broken connection, etc. They are mainly caused by energy overstress, rework cable during installation and rework connector, together with long heat exposure. It could result in moisture ingress, internalarcing and power loss.	
Diode fault	Common diode fault happens to the bypass diode (BPD), caused by excessive current level and improper or insufficient heat sinking. The lack of air flow in the junction box is also crucial to diode fault, particularly in the case of fast transitions shadow-sun-shadow. Burnt BPD could cause short or open circuit of the diode,and therefore different level of power loss.	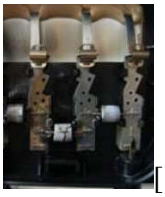 [

Burn mark	Partial shading + BPD fault or other mismatchfault (like low resistance defect in c-Si) could lead to energy consumption on the mismatched area instead of generation, therefore local high temperature of cell and induce burn mark. Besides, DC arc fault could also lead to burn mark. It may cause overheating, delamination or melting of material;	 [50]
Shunt hot spot	Partial shading could cause the cell turn to status of reverse biased voltage, to which thinfilm cells are extremely sensitive. Module current will concentrate on the shunt path and lead to hot spot. The behavior is quite different to c-Si hot spot as the BPD could not limit the reserved voltage. It is not likely to cause overheating but cause glass breakage and increase the risk of electrical shock.	 [51]

Table 2.3:Module-level faults

II.1.3 Array-level fault

At the array level, the main type of fault is the connection fault, which generally includes the earth fault, the line fault and the arc fault, as shown in Table II-3.

Fault	Description	Example
Ground fault (GF)	It is caused by un unintentional low impedance path between Current Carrying Conductor (CCC) and the ground get established. For *grounded* PV system, GF causes a high current to flow through an intentional circulating path. For *ungrounded* PV system, it generates residual magnetic field between the forward and backward current flow. It causes a change in insulation resistance and a lasting loss of power.	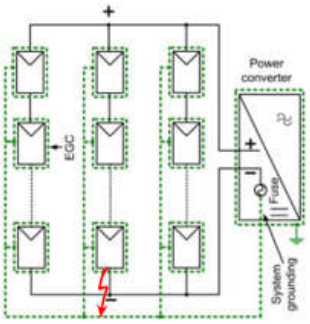
Line-line fault (LLF)	LLF rises from an unintentional low resistance path between two CCC with different electrical potential. It is caused by poor insulation of string connectors, accidental short-circuit between CCC, fault mounting, or external damage. It leads to high reverse current (depends on the potential difference of the location where the LLF happens) flowing to the faulty path and a lasting loss of power. LLF has 2 types, *intra-string,* and *cross-string* L	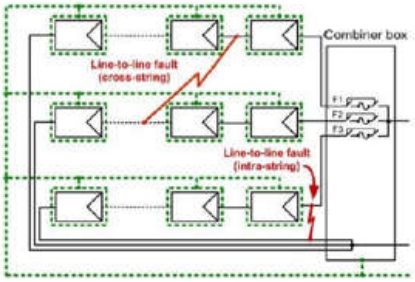
Arc fault (AF)	Several external factors could lead to the discontinuity or insulation fault of CCC and establish an air path for arc fault. Arc fault has two types: *series* and *parallel* AF (intra-string, cross-string and parallel to ground). It could occur in almost all the connection points or structures in the PV array, like cell, busbar, module, diode, string, safety devices, etc. It leads to transient but extremely high temperature that may burn the metal coating of the module. Besides, it generates highfrequency components causing serious nonlinear distortions in current and voltage.	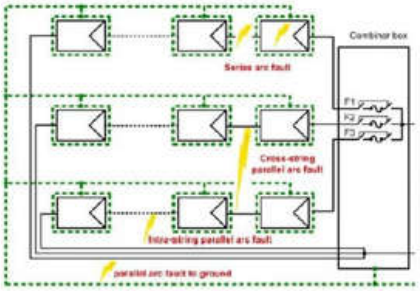

Table 2.4: Array-level faults

II.2 Fault Symptoms

In this section, we present faults while taking into account the impact of their severity on the behavior of a PV generator.

II.2.1 Mismatch and Shading Faults

The mismatch fault refers to the issue caused by grouping cells with non-identical I-V characteristics. Any variation in one of their parameters will lead to a discrepancy in their behavior. The shading fault is a particular case of mismatch fault, as it results in reduced sunlight exposure for some cells.

These parameter changes mainly stem from two factors:

- First, some cells may have different physical properties due to manufacturing tolerances.
- Second, PV cells may be subjected to different operating conditions caused by various faults, particularly those listed in Table II.4.

Fault	Symptoms
Shading	• Isc remains unchanged • Voc decreases when a significant number of cells are shaded • Fill factor decreases depending on the shading factor • Presence of an inflection point
Soiling	• Reduction of Isc depending on the transmission coefficient • Voc decreases when the transmission coefficient is very low •
Series Resistance	• Voc and Isc remain unchanged • Fill factor decreases as the value of Rs increases • Presence of an inflection point for a high Rs value • Slope deviation compared to the normal curve • Voc remains unchanged for low severity • Fill factor decreases as the normal value decreases.
Shunt Resistance	• Isc remains unchanged • Voc remains unchanged for low severity • Fill factor decreases as the value of Rp decreases • Slope deviation compared to the normal curve •
Temperature	• Isc remains unchanged • Voc and fill factor decrease as temperature increases.

Table 2.5: Symptoms of Mismatch and Shading Faults

II.2.2 Bypass Diode Fault

Under normal conditions, the bypass diode conducts when the sum of the voltages of the cells it protects becomes negative and remains non-conductive otherwise. When the diode is faulty, this protective role is no longer fulfilled. According to Table II.5, the electrical faults commonly associated with bypass diodes include:

- Short-circuited diode
- Disconnected (open) diode
- Reversed polarity diode

In addition to these electrical faults, the diode may also fail dynamically during operation and behave as an arbitrary impedance.

Figure 2.1 illustrates a schematic of a group of cells (j-th group) in which the bypass diode is replaced by an element that can simulate one of several faulty states: short circuit, open circuit, arbitrary impedance, or reversed diode.

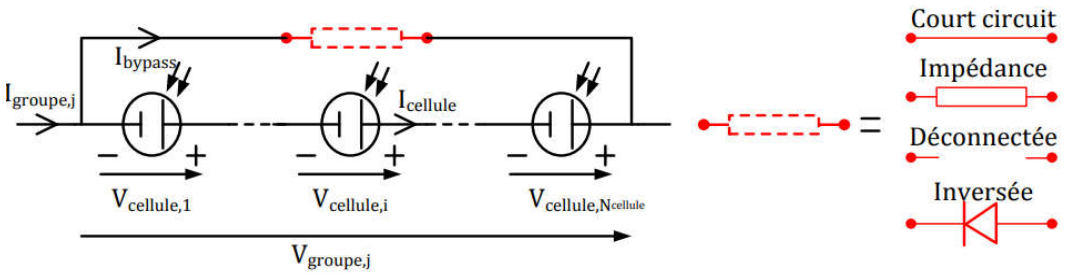

Figure 2.2: Block diagram of a PV cell group with a faulty bypass diode

Fault	Symptoms
short-circuit	• Isc remains unchanged • Voc decreases depending on the number of short-circuited diodes • The reduction in Voc is easy to quantify (-10V per diode) •
Open-Circuit	• Voc remains unchanged • Isc and fill factor (FF) decrease significantly depending on the number of shaded cells • Slope deviation compared to the normal I-V curve •
Reversed	• Voc decreases depending on the number of reversed diodes • Isc and fill factor (FF) decrease significantly depending on the number of shaded cells

Table 2.6: Different Fault States of a Bypass Diode

II.2.3 Module Fault

A module fault refers to all electrical faults associated with the connection of a module within a PV string. According to Table II.6, these electrical faults include:

- Short-circuited module
- Module connected in parallel with an impedance
- Module polarity reversal

Fault	Symptoms
Module	• **Isc remains unchanged** • **Voc decreases in the case of a short-circuit fault** • **Voc remains nearly unchanged for low shunt resistance values, but gradually decreases as the resistance decreases further** • **Slope deviation occurs in the case of shunted module faults**

Table 2.7: Different Symptoms of a Faulty PV Module

II.2.4 Connection Fault

A connection fault is related to the problem of increased contact resistance between two PV modules. Under normal operation, this contact resistance is nearly zero. However, this resistance can increase in several abnormal cases (such as corrosion of the connectors, loose screws, etc.). In extreme cases, an infinite resistance can be used to represent a module that is disconnected from the PV string.

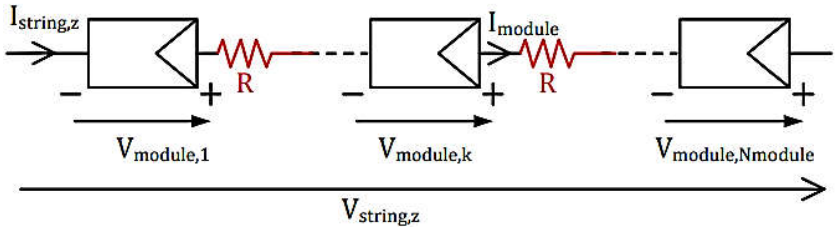

Figure 2.3: Block diagram of a PV string with non-zero connection resistance

II.2.5 Reverse Diode Fault

Similarly to the bypass diode, four types of faults can be considered for the reverse diode:

- short circuit,
- arbitrary impedance,
- open circuit, and
- reversed polarity.

Figure 2.3 shows a diagram of a PV field in which the reverse diode is replaced by an element that can represent, in each case, one of the diode's faulty states**.**

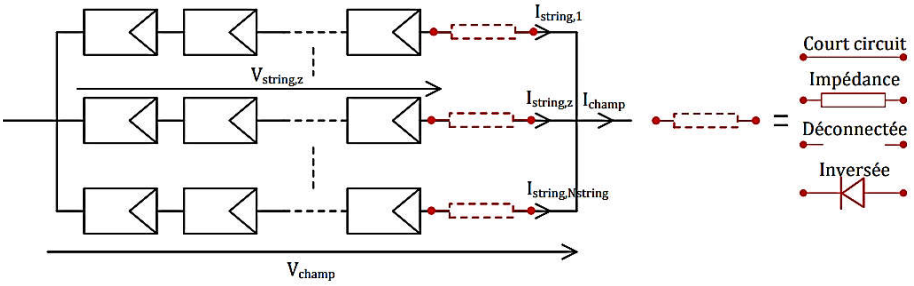

Figure 2.4: Block diagram of a PV field with a faulty reverse diode

II.2.6 Symptoms of PV Generator Faults

The symptoms evolve based on three main factors:

- Fault severity: As the magnitude of the fault changes, the symptoms vary accordingly.
- Operating conditions: Sunlight intensity significantly affects the manifested symptoms.
- Type of PV generator: The effect of a fault differs for a single-module PV, a string, or a PV array.

In this study, we focus on five symptoms that frequently appear at the PV generator level, as shown in tableII.7. The selection of these symptoms is a crucial step for the success of any diagnostic algorithm.

Condition	Impact on I-V curve	Examples
Healty	**None**	
Partial Shading (PS) **1 Module**	**Appearance of an inflection point** The voltage change at the inflection point occurs at about 2/3 of V_{OC} under healthy condition since there are three modules in one string while one module is shaded; **larger the PS degree, lower is the current of the inflection point.**	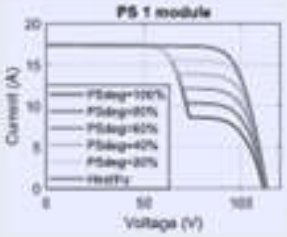
Short Circuit (SC) **1 Module**	**Voltage decreases** The V_{OC} on SC curve decreases by 1/3 of V_{OC} in healthy condition since one out of three modules is SC.	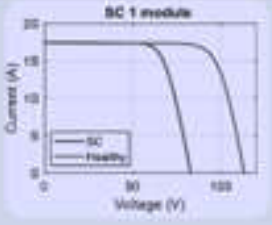
Open Circuit (OC) **1 String**	**Current decreases** The I_{SC} on OC curve decreases by 1/2 of I_{SC} in healthy condition since one out of two strings is OC.	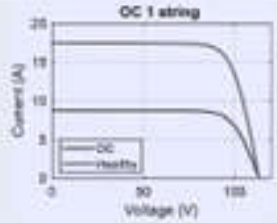
R_s degradation	**Slope decreases in the voltage region.** The greater the value of the added resistance is, the smaller the slope in the voltage area is.	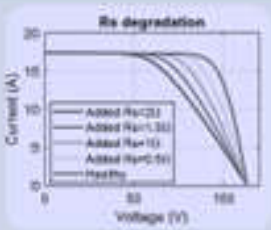
R_{sh} degradation	**Slope increases in the current region** The smaller the value of the added resistance is, the greater the slope is.	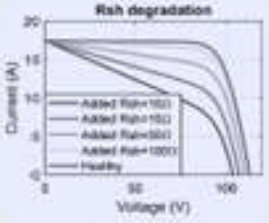

Table 2.8: Commonly Observed Symptoms at the PV Generator Level

Simulation studies of the behavior of a PV module under the considered faults have shown that it is possible to identify potential symptoms that can be used to trace back to the nature of the faults. A given fault may generate one or multiple symptoms, but some symptoms are

common to several faults. Therefore, the combination of identified symptoms—also referred to as fault signatures—makes it possible to identify the fault or a group of faults responsible for the observed behavior.

As an example, comparing the I-V characteristic of a faulty PV generator with that under normal operation can help identify potential symptoms for diagnostic purposes (see Table II.7).

II.3 Diagnostic Methods

Several diagnostic methods are reported in the literature, including:

- Infrared method
- Electrical method
- Reflectometry method
- Operating point analysis method

II.3.1 Infrared Method

There are several non-electrical diagnostic methods, either destructive or non-destructive, for detecting faults at the solar cell level. The main fault that can occur at this level is cell cracking within the photovoltaic module. The infrared imaging method (thermal camera) is widely applied.

This method is based on the principle that all materials emit infrared radiation within a wavelength range that depends on the material's temperature. By examining the temperature distribution across the module, any anomalies (if present) can be located.

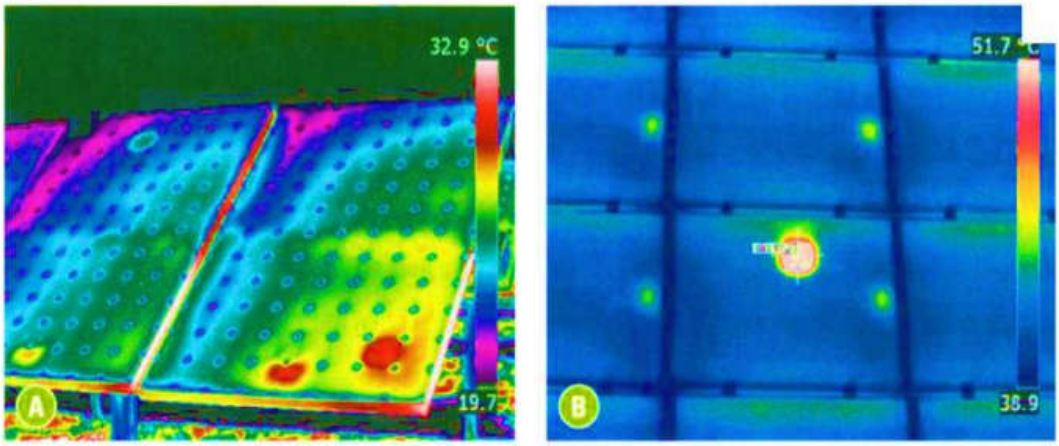

Figure 2.5: Example of Fault Detection Using Infrared Thermography

II.3.2 Electrical Method

Current PV system monitoring tools are mainly integrated into inverters. In this context, the most commonly measured parameters are:

- The current delivered by the PV array
- The voltage across the PV array

- The insulation resistance between the positive and negative terminals of the PV array

It is also possible to add complementary parameters such as the ambient temperature of the site and solar irradiance to the electrical measurements. These additional data require specific sensors (a temperature probe and a reference cell). If these parameters are needed, they should be processed using a dedicated controller (PLC). This controller is connected to the inverter and centralizes all the data in order to store them and/or send them to a remote server.

II.3.3 Reflectometry Method

The electrical reflectometry method is an electrical technique that allows measurement of the electrical characteristics of a transmission line and detection of any discontinuity points. Reflectometry is commonly used to determine the electrical state of cables and lines. It provides information for fault detection, location, and characterization.

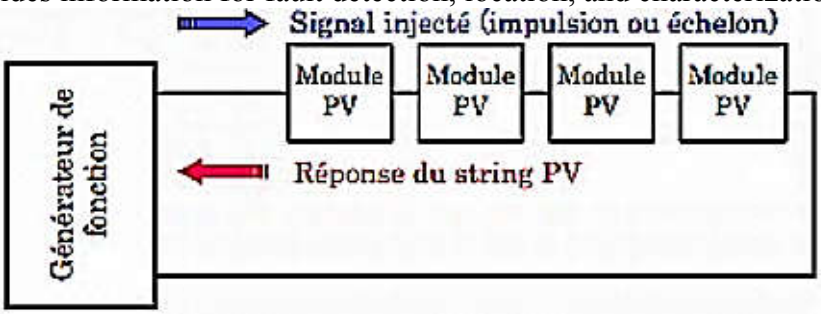

Figure 2.6. Principle of reflectometry for locating a fault in a PV string

II.3.4 Operating Point Analysis Method

The comparison between the measured maximum power and the simulated one can provide more information about the behavior of the PV generator. The main idea is to identify the type of fault present in a PV installation, particularly in the PV generator. These faults are grouped into four categories:

- Faulty modules in a string
- False alarm
- Faulty string
- Shading, aging, MPPT error

III. Conclusion

In this chapter, we presented the various faults affecting PV panels. We showed that these faults can generally be divided into manufacturing defects and those due to climatic and operational conditions. We also observed that most so-called electrical faults are caused by climatic conditions, such as the increase in series resistance. Finally, we introduced some basic concepts regarding diagnostic methods for photovoltaic panels.

Chapter 3

Modelling and simulation

I. Introduction

The primary objective of this third chapter is to establish a generalized mathematical model capable of representing the operational characteristics of a photovoltaic (PV) module in both healthy and faulty states. Building upon Bishop's well-known model, we have developed distinct sub-models, each specifically designed to characterize a particular type of fault. This research focuses on seven prevalent fault conditions in PV modules. The methodology involves presenting each sub-model individually, followed by the development of a comprehensive model that integrates all seven fault conditions under consideration. A subsequent simulation study will be conducted to rigorously validate the accuracy of the proposed model.

II. Mathematical Model of a PV Module in a Healthy State

II.1 PV cell model

The simplest PV cell model uses a single diode model (SDM) or double diode model (DDM) to represent the PV cell behavior, but these models often falls short in capturing real-world phenomena like the breakdown behavior at high reverse voltages. Bishop's model extends the single diode model by incorporating an additional breakdown mechanism to improve the accuracy of modeling PV cells, especially under reverse bias.

Bishop's model not only serves as a fundamental tool for PV cell characterization and simulation but also provides a framework for analyzing performance losses and identifying faults. It is widely implemented in simulation software and analytical studies, making it a powerful and reliable model for both researchers and engineers. By integrating realistic circuit elements and adapting to abnormal operating conditions, the Bishop model remains a cornerstone for understanding PV cell performance in practical and faulty scenarios.

According to its electrical equivalent circuit illustrated in Figure 3.1, the Bishop's model can be mathematically expressed by Equation 3.1:

$$I = I_{ph} - I_o\left(\exp\left(q\frac{V_d}{AkT}\right) - 1\right) - \frac{V_d}{R_{sh}}\left(1 + M(V_d)\right) \quad (3.1)$$

With$M(V_d)$ as the multiplier factor, expressed by Miller's formula.

$$M(V_d) = 1 + a\,\frac{V_d}{R_{sh}}\left(1 - \frac{V_d}{V_{br}}\right)^{-n} \quad (3.2)$$

and

$$V_d = V + R_s I \quad (3.3)$$

Where$I_{ph}$is the light-generated current (or photocurrent), I_o is the reverse saturation current, R_s and R_{sh} denote, the series resistance and the shunt resistance,q is the electron charge (q =1.602 × 10^{-19} C), A is the ideality factor and k is the Boltzmann's constant (k=1.38 × 10^{23} J/K). V_{br} is the junction breakdown voltage, a is the fraction of ohmic current involved in avalanche breakdown, and n the avalanche breakdown exponent.

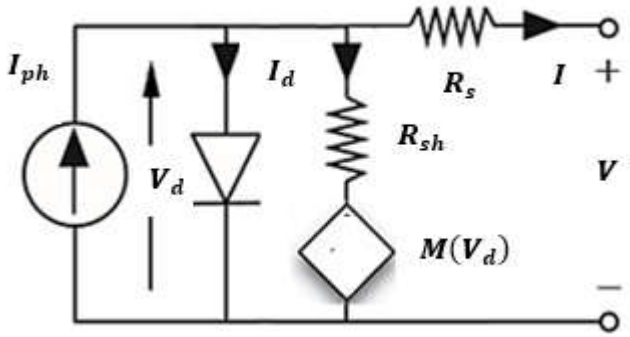

Figure 3.1. Electrical Equivalent Circuit of Bishop's Model

By rearranging its equivalent electrical circuit, the Bishop model can be represented by the electrical circuit in Figure 3.2 and, mathematically, by Equation 3.4.

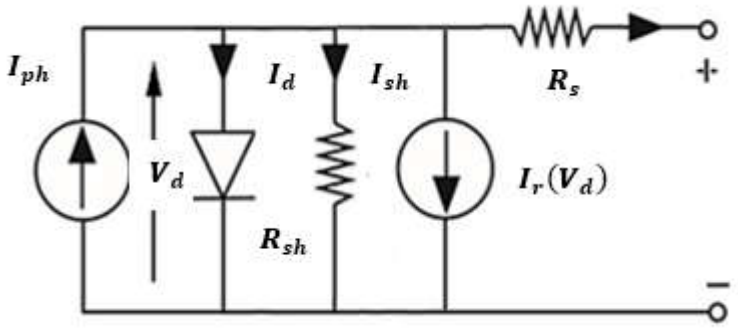

Figure 3.2. Another Representation of Bishop's Model Equivalent Electrical Circuit

$$I = I_{ph} - I_o\left(\exp\left(q\frac{V+R_sI}{AkT}\right)-1\right) - \frac{V+R_sI}{R_{sh}} - a\,\frac{V+R_sI}{R_{sh}}\left(1-\frac{V+R_sI}{V_{br}}\right)^{-n} \qquad (3.4)$$

Usually,I_o,A,I_{ph},$R_s$andR_{sh}areprovided by manufacturerasdata valid underStandardTestConditions(STC),i.e.spectrumAM1.5,irradianceG*=1000W m^{-2}andcelltemperatureT*=25°C.However, at any arbitrary operating condition (AOC) different to STC, these parameters vary, therefore, we must have recourse to other additional equations expressing each of the five parameters as a function of cell temperature and total absorbed irradiance. In this sense, various models have been reported in literature. The most developed and commonest equations describing the photocurrent I_{ph} and the reverse saturation current I_o variation with respect to the weather parameters (irradiance and cell temperature)arelistedrespectivelyinEqs.(3.5)and(3.6).Thefirstone(I_{ph})dependslinearly onthereceivedirradiancewithslighttemperature correction and the second one (I_o) varies strongly with the cell temperature.

$$I_{ph} = \propto_G \left(I^*_{ph} + \mu_{Isc}(T - T^*)\right) \qquad (3.5)$$

$$I_o = I^*_o\left(\frac{T}{T^*}\right)^3 \exp\left(\frac{qE_g}{Ak}\left(\frac{1}{T^*}-\frac{1}{T}\right)\right) \qquad (3.6)$$

In the above equations, α_G=G/G* denotes the irradiance coefficient, which actually represents the rate of the change of the irradianceG withrespecttotheirradianceatSTC.I^*_{ph}(≈I^*_{sc}),I^*_oandT*arethephotocurrent,there versesaturationcurrentandthe cell temperature at STC, respectively. $I_{\mu Isc}$ is the

temperature coefficient of the short-circuit current.

Theband gap energy E_g is nearly a linear function of cell temperature. At reference temperature T*=298K, E^*_g=1.121eV for silicon cell. It might be accounted for all of silicon solar cells by means of the following expression.

$$E_g = E_g^*\left(1 - 0.0002677\,(T - T^*)\right) \tag{3.7}$$

The dependence of the solar cell shunt resistance R_{sh} with respect to environmental parameters (solar irradiance and cell temperature)iswidelyreportedintheliterature.Mostofthemproposethesameempiricalexpression,inwhichtheshunt resistance is approximately inversely proportional to absorbed irradiance. Unfortunately, this approach is only valid for very low irradiance levels (i.e. for G ≈0). Hence, it does not offer possibilities to simulate the electrical behavior of PV devices under inhomogeneous weather conditions (ex: PV module with solar cells fully shaded, i.e. G =0).

Besides the aforementioned one, another empirical expression describing the irradiance dependence of PV modules shunt resistance as an exponential function is suggested by the well-known commercial software for design and simulation of photovoltaic systems 'PVsyst'. Such model includes an option to vary R_{sh} with irradiance ranging from 0 to 1000Wm^{-2}. Since the PVsyst's model is the only one that can be used for a wide range of solar irradiance, it is adopted in our study.

As the PVsyst's model calculating the shunt resistance is established for the PV module, in our study, we have rewritten it for a single PV cell, in which the shunt resistance can be calculated according to the following formula.

$$R_{sh} = R_{sh}^* + (R_{sho} - R_{sh}^*)\exp(-5.5 \propto_G) \tag{3.8}$$

Where the values of the cell shunt resistance R∗ at STC and Rsho corresponding to G = 0 can be derived from those of the PV module so, the pair (R∗ ,R_{sho}) can be determined as follows:

$$R_{sh}^* = \left(\frac{p}{s}\right) R_{shM}^* \tag{3.9}$$

$$R_{sho} = \left(\frac{p}{s}\right) R_{shoM} \tag{3.10}$$

As for the series resistance R_s and the ideality factor, most authors treat them as independent of the incident irradiance and cell temperature. Therefore, these parameters are given with respect to STC parameters as follows.

$$R_s = R_s^* \tag{3.11}$$

$$A = A^* \tag{3.12}$$

II.1.1 PV module model

Like any photovoltaic module, it consists of a set of cells connected in series and equipped with at least one by-pass diode to protect the module against mismatch effects, shading, hot-spots, etc (see Figure 3.3) . The equations describing a PV module are as follows:

- Equation$I_M(V_M)$ of the PV module:

$$I_M = I_{phM} - I_{oM}\left[\exp\left(q\frac{V_M + IR_{sM}}{AkT}\right) - 1\right] - \frac{V_M + I_M R_{sM}}{R_{shM}} - a\frac{V_M + I_M R_{sM}}{R_{shM}}\left(1 - \frac{V_M + I_M R_{sM}}{V_{br}}\right)^{-n} \tag{3.13}$$

- Equation IBP(VBP) de la diodoe de by-pass

$$I_{BP} = I_{oBP}\left[\exp\left(q\frac{-V_{BP}}{mkT}\right) - 1\right] \tag{3.14}$$

Where:

V_M and I_M are respectively the voltage and current of the PV module (with $V_M=n_s\cdot V$, $I_M=I$), RsM and R_{shM} are respectively the series and parallel resistances of the module (with $R_{sM}=n_s\cdot Rs$, $R_{shM}=n_s\cdot R_{sh}$)

V_{BP} and I_{BP} are respectively the voltage and current of the by-pass diode and I_{oBP} is the reverse saturation current of the by-pass diode.

.

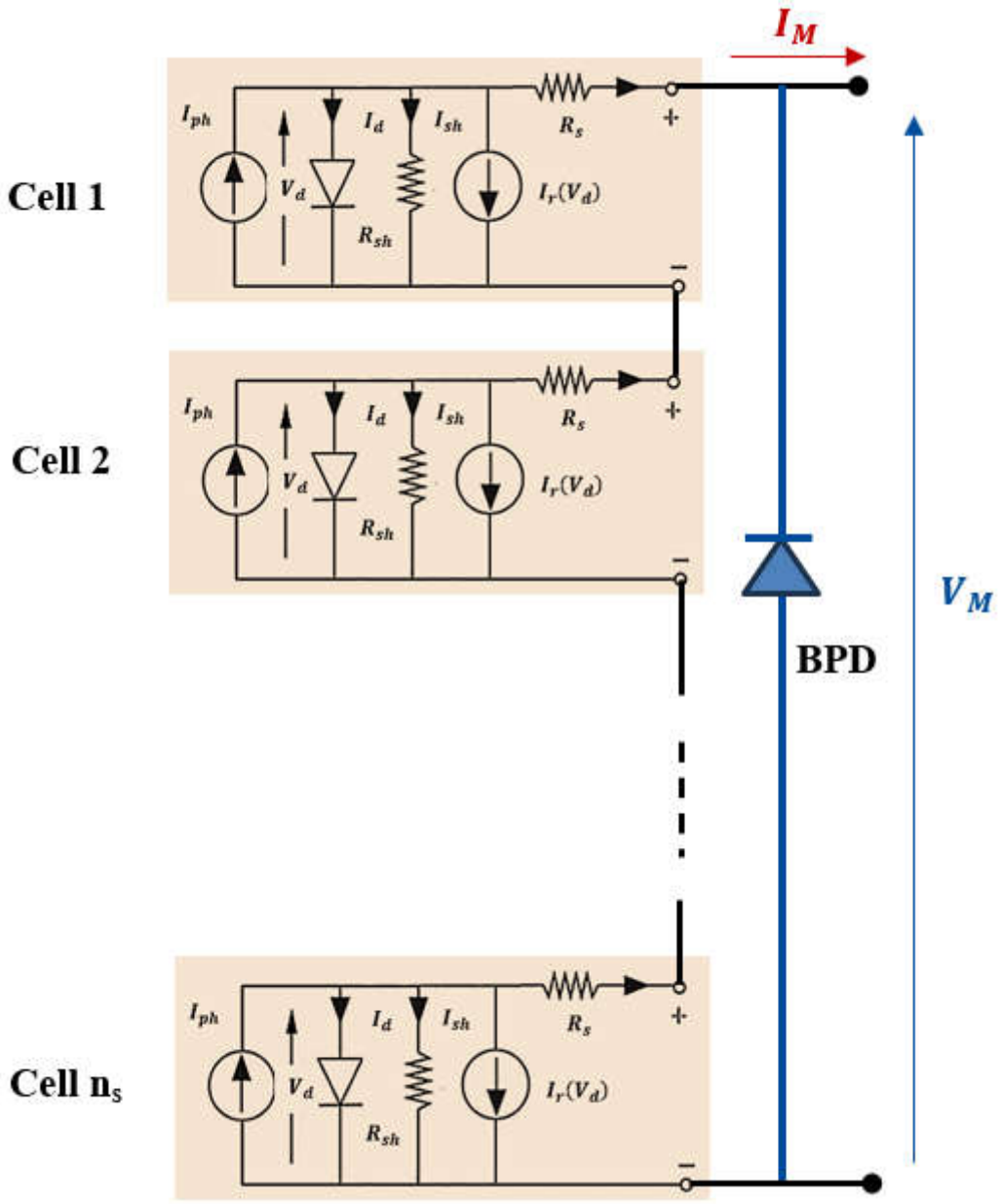

Figure 3.2. Equivalent Electrical Circuit of a PV Module

II.1 Mathematical Sub-model of the Faulty Module

II.1.1 Sub-model for the Partial Shading Fault

When modeling the impact of shading, only the **shading coefficient (k_{sh})** is integrated into Equation (3.2). This coefficient quantifies the extent of shading, ranging from k_{sh}=1 for a fully shaded module to k_{sh}=0 for a completely unshaded (fully sunlit) module. The effect of k_{sh} is exclusively applied to the **photogenerated current**, as it is directly proportional to the incident

solar irradiance, which is diminished by shading. Consequently, as shading increases, the photogenerated current proportionally decreases. This specific sub-model, capturing the behavior under partial or full shading, is accurately described by the following relation:

$$I_M = (\mathbf{1 - k_{sh}})\, I_{ph} - I_{oM}\left[\exp\left(\frac{V_M + IR_{sM}}{m\, v_t}\right) - 1\right] - \frac{V_M + I_M R_{sM}}{R_{shM}} - a\,\frac{V_M + I_M R_{sM}}{R_{shM}}\left(1 - \frac{V_M + I_M R_{sM}}{V_{br}}\right)^{-n} \quad (3.15)$$

II.1.2 Sub-model of Fault due to Soiling and Dust

The phenomenon of soiling and dust accumulation on the surface of a photovoltaic (PV) module is defined as the formation of an occluding layer that hinders the transmission of solar light. This layer is characterized by a **transmission coefficient (k_{tr})**, whose value directly depends on the thickness and density of the deposited layer. This coefficient ranges from zero (indicating zero transmission for an extremely thick or opaque layer) to a value close to 0.9 (representing a very light layer allowing nearly complete transmission). The impact of this soiling phenomenon manifests exclusively on the module's **photogenerated current (I_{phM})**, which is directly proportional to the effective solar irradiance reaching the cells. Thus, k_{tr} acts as a multiplicative reduction factor on I_{phM}. This sub-model, which captures the performance losses due to soiling, is formulated by the following relation, integrated into Bishop's model equation:

$$I_M = K_{tr}\, I_{ph} - I_{oM}\left[\exp\left(\frac{V_M + IR_{sM}}{m\, v_t}\right) - 1\right] - \frac{V_M + I_M R_{sM}}{R_{shM}} - a\,\frac{V_M + I_M R_{sM}}{R_{shM}}\left(1 - \frac{V_M + I_M R_{sM}}{V_{br}}\right)^{-n} \quad (3.16)$$

II.1.3 Sub-model of Fault due to Mismatch

The mismatch fault is a phenomenon caused by the grouping of photovoltaic (PV) cells possessing non-identical current-voltage (I-V) characteristics. Any variation in one of the fundamental parameters of Equation 3.1, which describes the cell model, will lead to a dissimilarity in their individual characteristics. Within the scope of our study, we have chosen to consider two main types of mismatch faults: the fault due to the dispersion of series resistance and the fault due to the dispersion of parallel resistance.

In the first case, that of series resistance, the behavior of the I-V characteristic is studied when the series resistance parameter increases by a value k_{m-rs}. This increase can be the consequence of potential oxidation of metallic contacts or issues with the module's internal

wiring. As for the mismatch fault due to parallel resistance, it manifests as a decrease in the parallel resistance by a certain value k_{m-rsh}. This decrease can be caused by microcracks or manufacturing defects creating leakage paths. In this mismatch sub-model, other parameters, such as the shading coefficient (k_{sh}=0) and the soiling transmission coefficient (k_{tr}=0), are considered to have no effect, meaning the module is neither shaded nor soiled. Thus, this mismatch sub-model can be expressed by the following relation, based on the modified single-diode model:

$$I_M = \boldsymbol{I_{ph}} - I_{oM}\left[\exp\left(\frac{V_M + I_M(\boldsymbol{R_{sM}} + \boldsymbol{k_{m-rs}})}{mv_t}\right) - 1\right] - \frac{V_M + I_M(\boldsymbol{R_{sM}} + \boldsymbol{k_{m-rs}})}{(\boldsymbol{R_{shM}} - \boldsymbol{k_{m-rsh}})} - a\,\frac{V_M + I_M(\boldsymbol{R_{sM}} + \boldsymbol{k_{m-rs}})}{(\boldsymbol{R_{shM}} - \boldsymbol{k_{m-rsh}})}\left(1 - \frac{V_M + I_M(\boldsymbol{R_{sM}} + \boldsymbol{k_{m-rs}})}{V_{br}}\right)^{-n} \quad (3.17)$$

II.1.4 Sub-model of Fault due to Bypass Diodes

Under normal operating conditions, a bypass diode is designed to conduct (forward-biased) when the sum of the voltages of the cells it protects becomes negative, indicating that the cells are reverse-biased. Conversely, it remains blocked (non-conducting) when the cells generate a positive voltage. If the diode fails, its protective function is compromised, which can lead to irreversible damage to the cells.

The main electrical faults associated with this diode include a **short-circuited diode, a disconnected diode (open circuit), and a reversed diode**. In addition to these well-defined failure modes, a faulty diode may also experience partial breakdown during operation, behaving like an impedance with variable or unexpected values. For each failure case, it is essential to analyze the diode's behavior when it is short-circuited, open-circuited, exhibits arbitrary impedance, or is connected in reverse.

a) Short circuited Bypass Diode Fault

In the case of a short-circuited bypass diode, the voltage across the cell group it protects is almost entirely reduced to zero. The current flowing through this cell group of the photovoltaic module becomes the sum of the current produced by the cells themselves and the current flowing through the short-circuit path created by the faulty diode. The current generated by the cells is equal to their maximum output, while the short-circuit path carries the excess current. In this sub-model, the following relationship is used to describe the behavior of the bypass diode voltage:

$$V_{BP} = (R_{BP}\, I_{BP} + V_{oBP})k_{BP} \quad (3.18)$$

With $k_{BP} = 0$; $V_M = 0$

a) Open circuited Bypass Diode Fault

The group voltage equals the sum of the voltages of the cells within the group. The group current is equal to the current flowing through the string of cells.

$$V_{BP} = (R_{BP}\, I_{BP} + V_{oBP})k_{BP} \quad (3.19)$$

With $\boldsymbol{k_{BP} = 1}$; $I_{BP} = 0$; $V_M = V_{oBP}$

b) Reversed BypassDiode Fault

Unlike a correctly functioning bypass diode, which conducts when the protected cells are reverse-biased (negative voltage) and blocks when they are forward-biased (positive voltage), **a reversed bypass diode** conducts **incorrectly**: it **blocks under reverse bias** and **conducts under forward bias**, behaving oppositely to its intended function.

In this faulty scenario, **the diode conducts even when the protected cells are forward-biased (i.e., producing power), thereby causing energy loss and possible heating.** This abnormal behaviour is usually caused by an **incorrectly installed** or **defective** diode (i.e., reversed polarity during installation).

$$V_{BP} = (R_{BP}\, I_{BP} + V_{oBP})k_{BP} \quad (3.20)$$

With $\boldsymbol{k_{BP} = -1}$

II.2 Mathematical Generalized Models for Faulty Modules

The proposed model provides a generalized mathematical framework that integrates multiple fault conditions commonly observed in photovoltaic (PV) modules. It extends **Bishop's model** by incorporating seven distinct fault factors: **partial shading, soiling, series resistance mismatch (Rs mismatch), shunt resistance mismatch (Rsh mismatch), and the effects of bypass diodes**. The parameters$\boldsymbol{k_{sh}}$, $\boldsymbol{k_{tr}}$, and $\boldsymbol{k_{BP}}$ serve as scaling or correction factors that adjust the photocurrent and voltage to account for the impacts of shading, soiling, and bypass diode operation, respectively. Additionally, the terms involving $\boldsymbol{k_{m\text{-}rs}}$ and $\boldsymbol{k_{m\text{-}rsh}}$ represent deviations in series and shunt resistances due to mismatch faults among modules or cells. These mismatches can result in increased power losses and the formation of hotspots. By adapting key parameters to reflect such non-idealities and failure conditions, the model enables more accurate and fault-resilient simulation of PV module behavior under real-world operating scenarios.

$$I_M = \boldsymbol{k_{tr}}(\mathbf{1} - \boldsymbol{k_{sh}})I_{\boldsymbol{ph}} - I_{oM}\left[\exp\left(\frac{V_M + I_M(\mathbf{1} + \boldsymbol{k_{m-rs}})R_{sM}}{m\, v_t}\right) - 1\right] - \frac{V_M + I_M(\mathbf{1} + \boldsymbol{k_{m-rs}})R_{sM}}{(\mathbf{1} - \boldsymbol{k_{m-rsh}})R_{shM}} \quad (3.21)$$

$$V_{BP} = (R_{BP}\, I_{BP} + V_{oBP})\boldsymbol{k_{BP}}$$

II.3 Simulation Study, Resultsand Discussion

To elucidate the various effects of fault indicator parameters, we implemented the model developed from equation 3.21 and conducted a simulation study using Matlab/Simulink software. In its block diagram form, this model is composed of four interconnected blocks (see Figure 3.4):

- The climatic parameters (irradiance, in W/m^2, and temperature, in K) and fault indicator parameters serve as inputs. These include: the shading factor (k_{sh}= 0÷1), the transmission coefficient (k_{tr}=0÷0.9), the mismatch parameter of the series resistance type ($k_{m\text{-}rs}$ = 0÷1), the mismatch parameter of the parallel resistance type ($k_{m\text{-}rsh}$ = 0÷1), and the parameter indicating the fault of the bypass diode (short-circuited diode: k_{BP}=0; reversed diode: k_{BP}=1).
- The core or central block represents the mathematical model expressed by equation 3.21.The
- The output block allows the visualization of results in both graphical form (I–V curve) and numerical form (electrical parameters: V_{oc}, I_{sc}, P_{mp}, FF, and efficiency).

It should be noted that these default indicator parameters are introduced for each module in the form of vectors (see Table 3.1).

Table 3.1. Various Fault Indicator Parameters and Their Nature

	k_{sh}	k_{tr}	$k_{m\text{-}rs}$	$k_{m\text{-}rsh}$	k_{BP}
Healthy module (no fault)	0	0	0	0	0
Partial shading	]0 1[	0	0	0	0
Total shading	1	0	0	0	0
Dust or soiling	0	]0 0. 9[	0	0	0
Mismatch type R_s	0	0	]0 1[	0	0
Mismatch type R_{sh}	0	0	0	]0 1[	0
Bypass diode short circuited	0	0	0	0	0
Bypass diode open circuited	0	0	0	0	1
Reversed Bypass Diode	0	0	0	0	-1

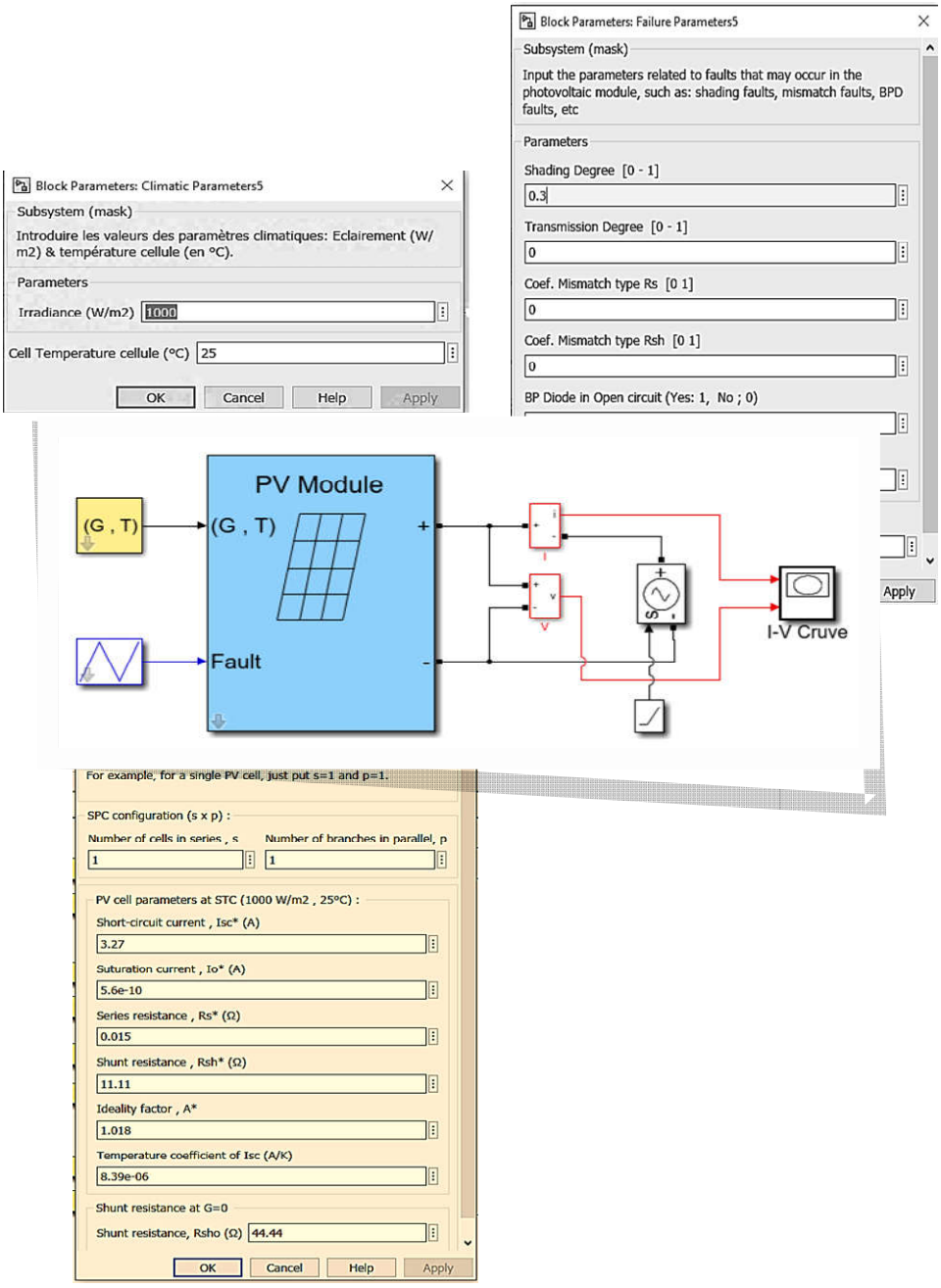

Figure 3.4. The proposed model in Simulink environment

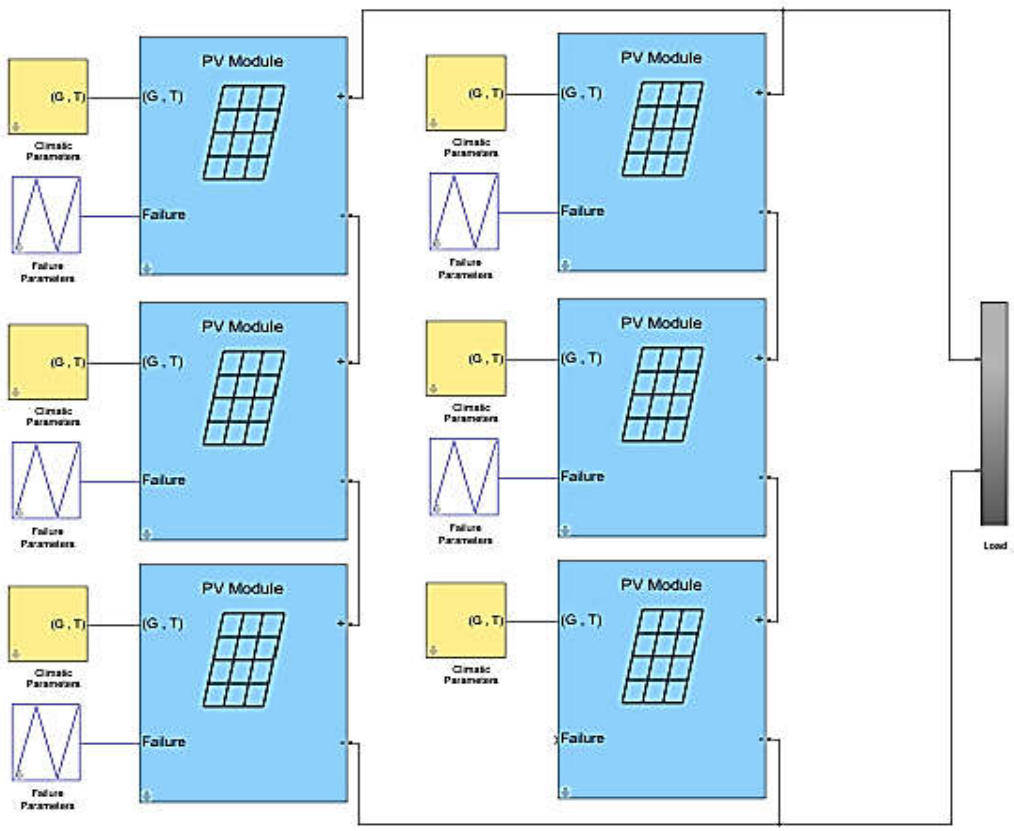

Figure 3. 5. Block diagram implemented in Simulink to generate the various faults.

To evaluate the effectiveness of the proposed method described above—which enables reproduction of the I-V curve—and to confirm its accuracy, a simulation study was conducted on a PV module with electrical characteristics specified under Standard Test Conditions (STC), as detailed in Table 3.3. This study examined various fault conditions using a 3x2 photovoltaic (PV) array configuration (two parallel strings, each consisting of three PV modules), simulated in MATLAB/Simulink.

Table 3.1.Electrical parameters of the PV module at STC.

Parameter	Variable	Value
Maximum power (W)	P^*_{mpM}	97.5
Voltage at maximum power (V)	V^*_{mpM}	15
Current at maximum power (A)	I^*_{mpM}	6.5
Short-circuit current (A)	I^*_{scM}	6.75
Open-circuit voltage (V)	V^*_{ocM}	19.83
Diode saturation current (nA)	I^*_{oM}	0.558
Diode quality factor	A^*	1
Shunt resistance (Ω)	R^*_{shM}	200
Series resistance (Ω)	R^*_{sM}	0.27
Shunt resistance at G=0 (Ω)	R^o_{shM}	800
Temperature coefficient of I_{sc}(mA/°C)	μ_{Isc}	2.3
Temperature coefficient of V_{oc} (mV/°C)	μ_{Voc}	-71.2

The results for the different scenarios are presented in the following sections.

II.3.1 Case of the fault due to shading

To study the effect of partial shading on the PV array under investigation, a fault indicator vector was introduced, in which only the degree or percentage of shading varies. In this case study, several scenarios wereconsidered:

- One module half-shaded (k = 0.5)
- Two modules in the same string shaded at 20%
- One string shaded at 70%
- Two modules in the same string shaded with different percentages

Figure 3.6 illustrates the I-V characteristics of a photovoltaic string under various partial shading conditions. It is evident that shading significantly affects the power output of the PV system. As the shading increases—either in terms of the percentage of surface area shaded or the number of shaded modules—the maximum power point (Pmp) decreases substantially.

For instance, in the absence of shading, the string achieves a **Pmp of 609 W**. However, when one module is half-shaded, the power drops to **469 W**. Further shading, such as two modules with 20% shading each, reduces the output to **526 W**. Severe shading, like 70% shading on a module, results in only **393 W**, and the same value is observed when two modules are shaded at different percentages.

These cases clearly indicate that both the extent and the distribution of shading critically affect power production.Moreover, the curves reveal that partial shading causes multiple steps or inflection points in the I-V characteristics, leading to multiple local maxima in the P-V curve. This makes maximum power point tracking (MPPT) more challenging under shaded conditions.

In summary, the more severe and uneven the shading, the greater the power loss. This underlines the importance of optimizing module placement and implementing shade-tolerant configurations or technologies in PV system design.

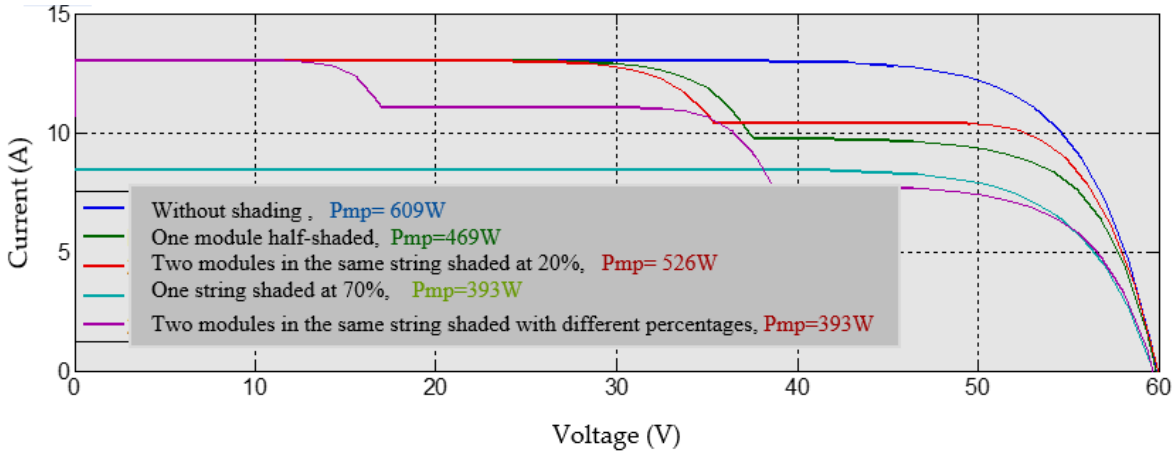

Figure 3.6. I-V Characteristics of the PV Array Under Normal and Various Partial Shading Conditions

II.3.2 Case of a Fault Due to Soiling and Dust

In this section, we studied the effect of dust and soiling on the same PV field illustrated in Figure 3.7. Two cases of the transmission coefficient were considered: k_{tr} = **0.2** and k_{tr} = **0.5**. We observe a reduction in short-circuit current and a slight variation in open-circuit voltage depending on the severity of the fault.

The two I-V curves shown in **Figure 3.7** represent the electrical behavior of a photovoltaic (PV) field under different levels of surface due to dust:

- **Blue Curve (Normal Conditions)**: This represents the normal operating condition without any soiling. It shows the highest short-circuit current (**Isc**) and open-circuit voltage (**Voc**), indicating optimal performance.
- **Green Curve (k_{tr}= 0.5)**: This corresponds to moderate soiling. The curve shows a noticeable decrease in I_{sc} while V_{oc} is only slightly reduced. This is typical of partial shading or contamination, where the light reaching the cells is attenuated but not completely blocked.
- **Red Curve (k_{tr} = 0.2)**: This reflects severe soiling. The reduction in I_{sc} is even more pronounced, with a further small drop in V_{oc}. This indicates significant loss of irradiance on the panel surface, reducing the photocurrent generated.

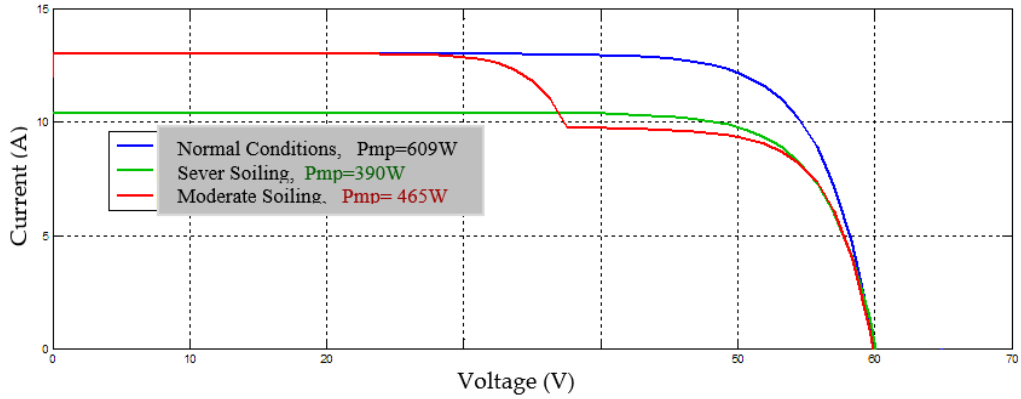

Figure 3.7. I-V Characteristics of the PV Array Under Normal and Different Degrees of Soiling

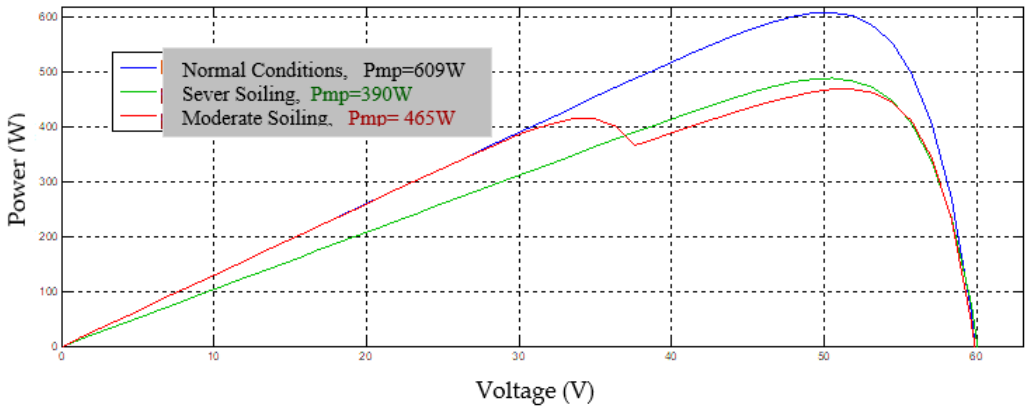

Figure 3.8. P-V Characteristics of the PV Array Under Normal and Different Degrees of Soiling

II.3.4 Case of a Fault due to Mismatch related to Series Resistance

In photovoltaic (PV) systems, **series resistance (Rs)** arises from internal resistive elements within modules and external connections. When one or more modules in a PV array have abnormally high Rs, it causes a mismatch that degrades the array's performance.

The I-V characteristics shown in **Figure 3.9** illustrate this effect clearly:

- Under **normal operation** (black curve), the array delivers optimal current and voltage, with a sharp knee in the I-V curve marking the **maximum power point (MPP)**.
- With **one module having Rs = 1 ohm** (blue curve), the impact is modest but noticeable. The I-V curve begins to curve downward earlier, leading to a **slight reduction in voltage and power output** at the MPP. This indicatesincreasedinternallosses.
- With **one module having Rs = 10 ohms** (red curve), the mismatch is severe. The I-V curve becomes much flatter, and the voltage drops significantly under load. This leads to a **substantial drop in both voltage and power output** at the MPP. The array'scurrent-carryingabilityisalsoreduced.

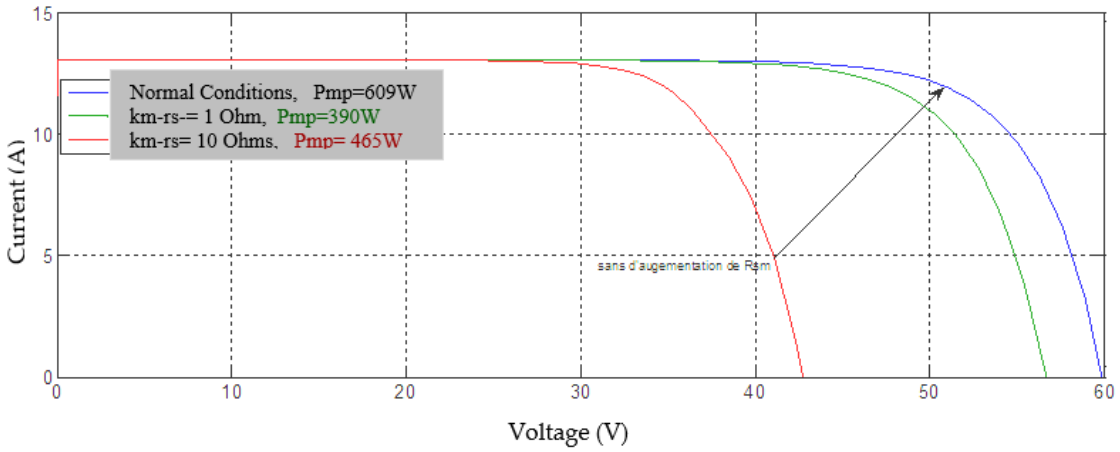

Figure 3.9. I-V Characteristics of a Photovoltaic Array under Normal Operation and in the Presence of a Mismatch Fault related to Series Resistance.

II.3.5 Case of a Fault due to Mismatch related to Shunt Resistance

This case presents the behavior of a photovoltaic array affected by a fault due to a mismatch in shunt resistance (R_{sh}). Shunt resistance represents unintended paths for current leakage inside the module. A decrease in R_{sh} indicates more current bypassing the load, which leads to power losses.

The simulation compares the I-V characteristics of:

- **Normal operation (high R_{sh})** – Green curve
- **Moderate degradation ($K_{m\text{-}rsh}$ = 109.9 Ω)** – Red curve
- **Severe degradation ($k_{m\text{-}rsh}$ = 10.95 Ω)** – Blue curve

The following conclusions can be drawn:

a. Short-circuit current (Isc) is unaffected

Regardless of the R_{sh} value, the current at zero voltage remains nearly constant.

This indicates that the initial current generation under illumination is notimpacted by the fault.

b. Open-circuit voltage (Voc) slightly decreases

As R_{sh} drops, the open-circuit voltage is marginally affected. A very low Rsh leads to a slightly lower Voc, but the drop becomes significant only at severe faults.

c. Major degradation in power output

The most critical impact is on the “knee” of the I-V curve, where power output is typically maximum (V_{mp}, I_{mp}). When Rsh is low:

- The I-V curve bends down earlier.

- The output power drops significantly.

d. Loss of Maximum Power Point (MPP)

With lower Rsh, the Maximum Power Point shifts down and left, making it difficult for MPPT algorithms to track it reliably. The module becomes inefficient, producing far less usable power.

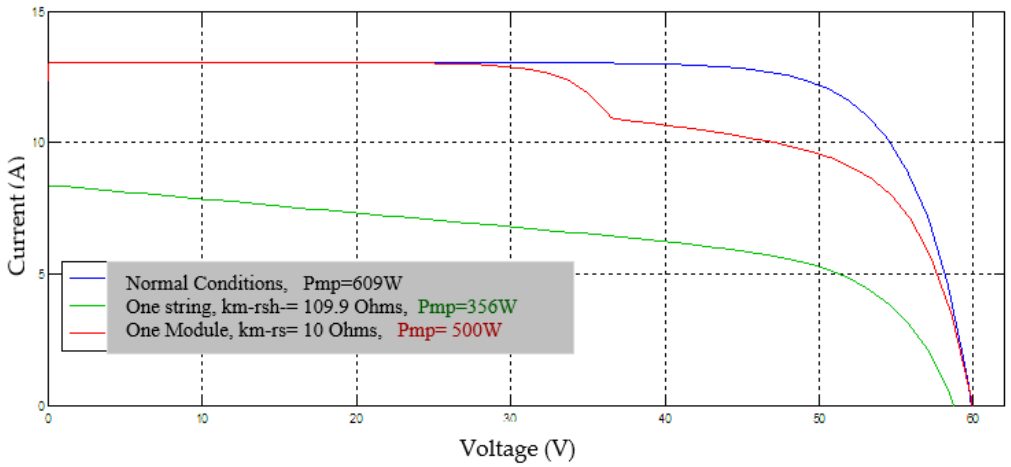

Figure 3.10. I-V Characteristics of a Photovoltaic Array under Normal Operation and in the Presence of a Mismatch Fault related to Shunt Resistance.

II.3.6 Case of a Fault due to Bypass Diode

a) Short circuited Bypass Diode

Figure 3.8 illustrates this case. Under normal operating conditions, the photovoltaic array achieves a maximum power point (Pmp) of 609 W, with a voltage at maximum power (Vmp) of approximately 42 V and a current at maximum power (Imp) of around 14.5 A.

However, when two bypass diodes are short-circuited—effectively removing the contribution of two modules—the I–V curve shifts significantly. In this fault condition, Vmp drops to approximately 19 V, while Imp remains close to 14.5 A, resulting in a reduced Pmp of about 275.5 W.This indicates a substantial power loss of more than 50%, emphasizing the critical impact of bypass diode failures on system performance.

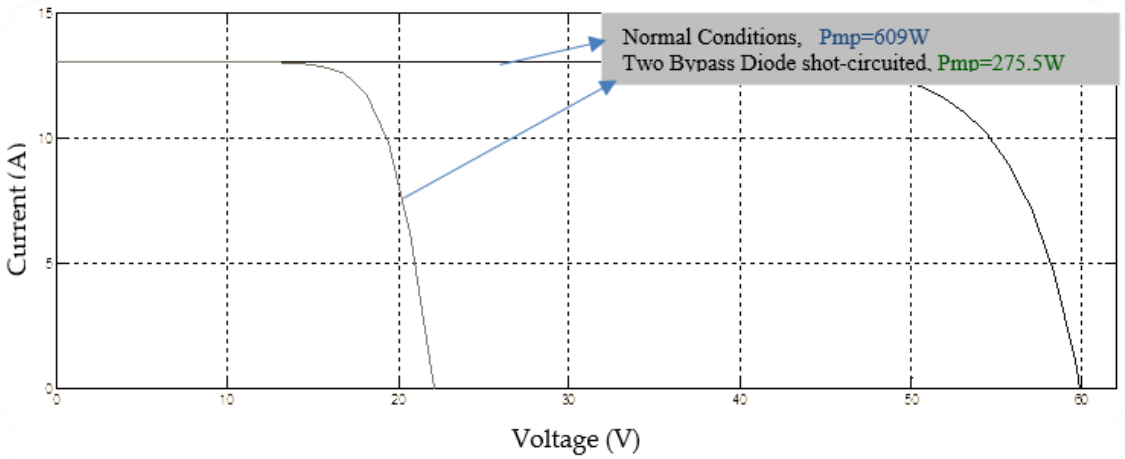

Figure 3.11. I-V Characteristics of a Photovoltaic Array under Normal Conditions and with a Fault due to Two Short-Circuited Bypass Diodes

b) Reversed Bypass diode

Figure 3.10 displays the I–V characteristics of a photovoltaic array under normal operating conditions and with a fault due to one reversed bypass diode. Under normal conditions, the array reaches a maximum power point (Pmp) of 609 W. When one bypass diode is reverse polarity, the I–V curve shifts, reducing the maximum output power. From the green curve, the maximum power point occurs at approximately 35 V and 11.25 A, resulting in a reduced Pmp of about 393.75 W. This corresponds to a power loss of around 35%, clearly demonstrating that even a single reversed bypass diode can significantly degrade system performance.

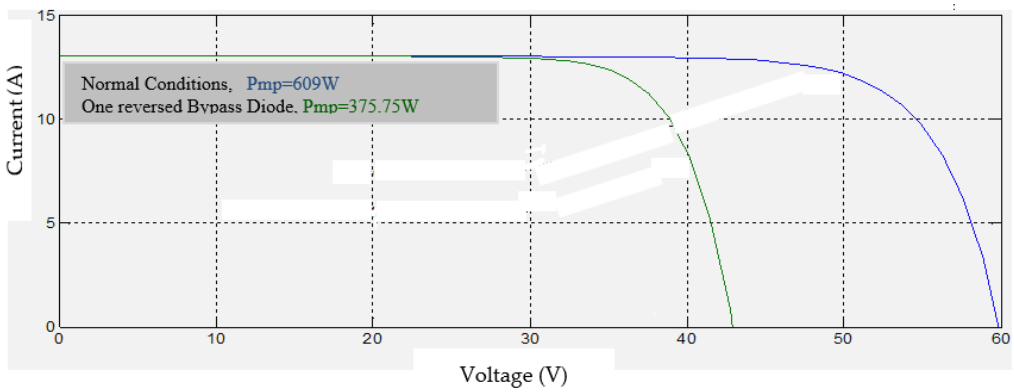

Figure 3.10. I-V Characteristics of a Photovoltaic Array under Normal Conditions and with a Fault due to One Reversed Bypass Diode

III. Conclusion

This chapter has developed a comprehensive mathematical model to simulate photovoltaic (PV) modules in both healthy and faulty conditions.Using Bishop's model as a foundation, various realistic parameters were integrated to reflect the effects of environmental factors and physical defects.Seven common fault types were individually modeled: partial shading, soiling, series and shunt resistance mismatches, and three bypass diode failures.Each fault sub-model alters the core electrical behavior of the PV module, demonstrating distinct impacts on the I–V and P–V characteristics.

A global fault model was then proposed, combining all indicators into a unified mathematical expression.This general model was implemented in Simulink, allowing dynamic simulations under different fault scenarios.

The simulation study validated the model's capacity to reproduce the behavior of real PV arrays under varying fault conditions.Results revealed significant losses in power output depending on the fault severity and type, particularly under shading and bypass diode issues.Mismatch in resistances led to subtle yet impactful variations, affecting maximum power tracking efficiency.Soiling predominantly reduced current, while diode faults caused abrupt voltage drops.

The I–V curves under faults displayed non-linearities, highlighting diagnostic complexity.This underscores the importance of robust modeling for accurate fault detection and performance prediction.

The proposed model enables more effective analysis, design, and monitoring of PV systems.

It can also aid in developing more reliable MPPT algorithms and fault-tolerant system designs.

Overall, Chapter 3 lays a solid groundwork for fault-aware PV modeling, essential for real-world deployment and maintenance strategies.

General Conclusion

This thesis has focused on the modeling and simulation of photovoltaic (PV) modules under the influence of commonly encountered faults such as partial shading, bypass diode failure, module mismatch, and surface contamination. By incorporating these anomalies into mathematical models, the study has demonstrated how various faults can significantly affect the electrical performance and I-V characteristics of PV modules.

The simulation results have highlighted the importance of accurate fault modeling in diagnosing performance degradation and optimizing system operation. Furthermore, the developed model can serve as a valuable tool for system designers, researchers, and maintenance engineers to detect and analyze faults efficiently, contributing to improved reliability and efficiency of PV systems.

Ultimately, this work emphasizes the critical role of advanced simulation techniques in enhancing fault tolerance and long-term sustainability of solar energy systems. Future studies may focus on real-time fault detection techniques and integrating machine learning approaches to automate the diagnostic process for large-scale photovoltaic installations.

Bibliographie

[ABETE'90] A. Abete, E. Barbisio, F. Cane and P. Demartini, "Analysis of photovoltaic modules with protection diodes in presence of mismatching," in Photovoltaic Specialists Conference, 1990., Conference Record of the Twenty First IEEE, 1990, pp. 1005-1010 vol.2.

[ADEME'06] ADEME, "Guide de spécifications techniques relatives à la protection des personnes et biens - Générateurs photovoltaïques raccordés au réseau," ADEME,2006.

[ALERS'11] G. B. Alers, "Photovoltaic Failure Analysis:Techniques for Microelectronics and Solar," in PV Module Reliability Workshop, Colorado, USA, 2011.

[ALONSO-GARCÍA'06] M. C. Alonso-García and J. M. Ruíz, "Analysis and modelling the reverse characteristic of photovoltaic cells," Solar Energy Materials and Solar Cells, vol. 90, pp. 1105-1120, 2006.

[ALONSO-GARCÍA'06] M. C. Alonso-García, J. M. Ruiz and F. Chenlo, "Experimental study of mismatch and shading effects in the I-V characteristic of a photovoltaic module," Solar Energy Materials and Solar Cells, vol. 90, pp. 329-340, 2006.

[ALONSO-GARCÍA'06] M. C. Alonso-García, J. M. Ruiz and W. Herrmann, "Computer simulation of shading effects in photovoltaic arrays," Renewable Energy, vol. 31, pp. 1986-1993, 2006.

[BARRUEL'10] F. Barruel, N. Chantreuil and A. Labrunie, "Procédé de diagnostic de la défaillance d'un générateur photovoltaïque," France Patent FR2944647 (A1), 2010-10-22, 2010.

[BISHOP'88] J. W. Bishop, "Computer simulation of the effects of electrical mismatches in photovoltaic cell interconnection circuits," Solar Cells, vol. 25, pp. 73-89, 1988.

[BP'11] "BP solar module," Available:

http://www.bpsolar.fr/solaire/panneau/panneau%20solaire.php

[BUN'11] L. Bun, B. Raison, G. Rostaing, S. Bacha, A. Rumeau, et al., "Development of a Real Time Photovoltaic Simulator in Normal and Abnormal Operations," in IECON 2011, 2011.

[CEC'97] CEC, "Guidelines for the Assessment of Photovoltaic Plants, Document B, Analysis and Presentation of Monitoring Data," Commission of the European Communities,1997.

[CHAO'08] K.-H. Chao, S.-H. Ho and M.-H. Wang, "Modeling and fault diagnosis of a photovoltaic system," Electric Power Systems Research, vol. 78, pp. 97-105, 2008.

[CHOUDER'10] A. Chouder and S. Silvestre, "Automatic supervision and fault detection of PV systems based on power losses analysis," Energy Conversion and Management, vol. 51, pp. 1929-1937, 2010.

[CLAVADETSCHER'07] L. Clavadetscher and T. Nordmann, "Cost and Performance Trends in Grid-Connected Photovoltaic Systems and Case Studies," Report IEA-PVPS T2-06, 2007.

[DALLAS'07] W. Dallas and et al., "Resonance ultrasonic vibrations for crack detection in photovoltaic silicon wafers," Measurement Science and Technology, vol. 18, p. 852, 2007.

[DE SOTO'06] W. De Soto, S. A. Klein and W. A. Beckman, "Improvement and validation of a model for photovoltaic array performance," Solar Energy, vol. 80, pp. 78-88, 2006.

[DÍAZ'07] P. Díaz, M. Á. Egido and F. Nieuwenhout, "Dependability analysis of stand-alone photovoltaic systems," Progress in Photovoltaic: Research and Applications, vol. 15, pp.245-264, 2007.

[DIAZ-DORADO'10] E. Diaz-Dorado, A. Suarez-Garci, C. Carrillo and J. Cidras, "Influence of the shadows in photovoltaic systems with different configurations of bypass diodes," in Power Electronics Electrical Drives Automation and Motion (SPEEDAM), 2010 International Symposium on, 2010, pp.134-139.

[DREWS'07] A. Drews, A. C. de Keizer, H. G. Beyer, E. Lorenz, J. Betcke, et al., "Monitoring and remote failure detection of grid-connected PV systems based on satellite observations," Solar Energy, vol. 81, pp. 548-564, 2007.

[DURU'06] H. T. Duru, "A maximum power tracking algorithm based on Impp=f(Pmax) function for matching passive and active loads to a photovoltaic generator," Solar Energy, vol. 80, pp. 812-822, 2006.

[EPIA'11] EPIA, "Solar generation 6," European Photovoltaic Industry Association, 2011.

[ESRAM'07] T. Esram and P. L. Chapman, "Comparison of Photovoltaic Array Maximum Power Point Tracking Techniques," IEEE TRANSACTIONS ON ENERGY CONVERSION, vol. 22, pp. 439-449, 2007.

[FEMIA'05] N. Femia, G. Petrone, G. Spagnuolo and M. Vitelli, "Optimization of perturb and observe maximum power point tracking method," Power Electronics, IEEE Transactions on, vol. 20, pp. 963-973, 2005.

[FIRTH'10] S. K. Firth, K. J. Lomas and S. J. Rees, "A simple model of PV system performance and its use in fault detection," Solar Energy, vol. 84, pp. 624-635, 2010.

[GOETZBERGER'98] A. Goetzberger, J. Knobloch and B. Voβ, Crystalline silicon solar cells: John Wiley & Sons, 1998

[GOW'09] J. A. Gow and C. D. Manning, "Development of a photovoltaic array model for use in power-electronics simulation studies," IEE. Proc.-Electr. Power Appl.,, vol. 146, 2009.

[HIBBERD'11] B. Hibberd, "PV Reliability & Performance - A project Developpers Experience," in Photovoltaic Module Reliability Workshop (NREL), Colorado, USA, 2011.

Abstract

Like any electrical or electronic system, a photovoltaic (PV) solar system may experience failures or degradation during operation. Several faults or anomalies can affect the PV generator (a set of PV modules), including issues such as module mismatch, partial shading, disconnection of bypass diodes (BPDs), accumulation of dust and dirt on the surface, short circuits, and more. These faults significantly impact the performance of the PV generator, often leading to changes in its I-V characteristics.

Mathematical modeling remains one of the most efficient, conclusive, and cost-effective methods for analyzing and studying the performance of an operational PV system. This Master's thesis aims to develop an analytical mathematical model that incorporates key parameters indicative of the most common faults in a PV module, providing a valuable diagnostic tool for PV systems.

Key words: Faults, diagnostic, symptoms.

Résumé

Comme tout système électrique ou électronique, un système solaire photovoltaïque (PV) peut subir des pannes ou une dégradation pendant son fonctionnement. Plusieurs défauts ou anomalies peuvent affecter le générateur PV (ensemble de modules photovoltaïques), notamment des problèmes tels que le désaccord entre modules, l'ombrage partiel, la déconnexion des diodes de dérivation (BPD), l'accumulation de poussière et de saleté à la surface, les courts-circuits, et d'autres encore. Ces défauts ont un impact significatif sur la performance du générateur PV, entraînant souvent des modifications de ses caractéristiques courant-tension (I-V).

La modélisation mathématique reste l'un des moyens les plus efficaces, concluants et économiques pour analyser et étudier les performances d'un système PV en fonctionnement. Ce mémoire de Master vise à développer un modèle mathématique analytique qui intègre les paramètres clés représentatifs des défauts les plus courants dans un module PV, fournissant ainsi un outil de diagnostic précieux pour les systèmes

Mots-clés: Défauts, Diagnostic, Symptômes

ملخص

هذه المذكرة عبارة عن عمل.يهدف إلى مثل أي نظام كهربائي أو إلكتروني، يمكن أن يتعرض نظام الطاقة الشمسية الكهروضوئية (PV) لأعطال أو تدهور أثناء التشغيل. هناك العديد من الأعطال أو الشذوذات التي قد تؤثر على المولد الكهروضوئي (وهو مجموعة من الوحدات الكهروضوئية)، بما في ذلك مشاكل مثل عدم تطابق الوحدات، التظليل الجزئي، فصل صمامات التجاوز(BPDs) ، تراكم الغبار والأوساخ على السطح، والدوائر القصيرة، وغيرها. تؤثر هذه الأعطال بشكل كبير على أداء المولد الكهروضوئي، مما يؤدي غالبًا إلى تغييرات في خصائص التيار-الجهد.(I-V)

تُعد النمذجة الرياضية من أكثر الطرق كفاءةً وفعاليةً من حيث التكلفة لدراسة وتحليل أداء نظام PVأثناء التشغيل. يهدف هذا البحث لنيل درجة الماستر إلى تطوير نموذج رياضي تحليلي يدمج المعلمات الأساسية التي تمثل أكثر الأعطال شيوعًا في وحدة كهروضوئية، مما يوفر أداة تشخيصية قيمة للأنظمة الكهروضوئية.

الكلمات المفتاحية : **عطب، تشخيص، أعراض.**